Higher-order conservative discretizations on arbitrarily varying non-uniform grids

A. Arun Govind Neelan[1†], Raimund Bürger[2*†], Manoj T. Nair[3†], Samala Rathan[4†]

[1]Department of Mechanical Engineering, Indian Institute of Technology-Madras, Chennai, 600036, Tamil Nadu, India.
[2*]CI[2]MA and Departamento de Ingeniería Matemática, Facultad de Ciencias Físicas y Matemáticas, Universidad de Concepción, Casilla 160-C, Concepción, Chile.
[3]Department of Aerospace Engineering, Indian Institute of Space Science and Technology, Thiruvananthapuram, 695547, Kerala, India.
[4]Department of Humanities Sciences, Indian Institute of Petroleum & Energy, Visakhapatnam, 530003, Andhra Pradesh, India.

*Corresponding author(s). E-mail(s): rburger@ing-mat.udec.cl;
Contributing authors: arunneelaniist@gmail.com; manojtnair@iist.ac.in; rathans.maths@iipe.ac.in;
†These authors contributed equally to this work.

Abstract

Conservative discretizations of transport equations are based on integral formulations that include the finite volume method (FVM) and conservative finite difference methods (CFDMs). The FVM is used by most fluid dynamics simulation packages and requires smoothly shifting grids for better convergence. This motivates the study of the order of accuracy and rate of convergence of the FVM on non-uniform grids. It is difficult to do such an analysis of the FVM on an unstructured grid; however, the FVM is reduced to a CFDM on a Cartesian grid. The effect of the order of accuracy and the rate of convergence of higher-order CFDMs on arbitrarily varying grids are investigated. It is shown that higher-order conservative discretizations on arbitrarily varying non-uniform grids need some smoothness in the grid transition to be first-order accurate. The condition to achieve first-order accuracy is also presented. If the grid is replaced by a gradually varying grid, it is shown that conservative discretizations yield a better rate

of convergence. In this situation, a rate of convergence between one and the theoretical maximum can be achieved in dependence on the grid stretch/contraction ratio. Numerical examples, including the linear convection-diffusion equation, the lid-driven cavity problem, and the Taylor-Green vortex problem, are presented.

Keywords: Finite volume method, finite difference scheme, conservative discretization, WENO, ENO

1 Introduction

The popular sub-classes of weighted residue methods to solve the governing equations of fluid dynamics are the finite volume method (FVM), finite difference method (FDM), and finite element method (FEM). The governing equations of fluid dynamics are typically in integral or differential form [1]. The FVM [2] uses an integral-based technique, the FDM employs a differential-based approach, and the FEM utilizes the weak form of the governing equation. Because of its conservativeness and ability to handle complicated geometries, the FVM is a common choice for fluid dynamics simulations. In practice, we use a finite-size mesh, so the integral-based approach may be preferred over the differential-based techniques. The FDM is extended to the integral formulation by volume averaging, which yields a conservative finite difference method (CFDM). Most of the weighted essentially non-oscillatory (WENO) schemes are based either on FVMs [3] or on CFDMs [4]. CFDM-based WENO schemes have the advantage that they are computationally less expensive than comparable FVM-based WENO schemes [5].

Usually, the performance of a scheme is measured based on the order of accuracy and rate of convergence. The rate of convergence refers to how quickly a convergent sequence approaches its limit or how rapidly an iterative algorithm approaches its solution. In numerical analysis and optimization, understanding the rate of convergence is crucial for evaluating the efficiency of algorithms. In other words, we can say it is the slope of a line drawn between the error in the numerical solution and the number of grids used in the log-log plot.

To find the order of accuracy of a numerical scheme, we should expand the computational molecule using Taylor's series. After that, we should find the co-efficient of the leading truncation error term, which will be a function of numbers and grid size. The numerical value of the power term of the grid size in the leading truncation error term defines the order of accuracy. This can also be written as the numerical value of the power term in grid size present in the leading truncation error term when we expand computational molecules in the finite difference formula using Taylor's series. Higher the order of accuracy, the numerical scheme satisfies higher-order derivative terms in the Taylor series expansion.

The rate of convergence and the order of accuracy are similar as long as the grid is uniform and the solution is smooth with some basic boundary conditions. However, to attain the desired rate of convergence, we need a certain degree of regularity of the grids on a non-uniform mesh [6]. On the other hand, some researchers claim that

the decrease in order of accuracy does not always imply a reduction in convergence rate [7–17]. Most of the above works contend that the relationship between the rate of convergence and the order of accuracy is weak. In fact, this situation may give rise to a super-convergence phenomenon where the rate of convergence exceeds the order of accuracy of the scheme [7, 8, 13]. In some circumstances, super-convergence occurs when the grid stretch/contraction ratio is carefully controlled.

The super-convergence phenomenon reported in [3] is associated with the presence of critical points in the solution. It is worth noting that critical points typically result in lower-order convergence, but in some circumstances, non-linear behaviour in the rate of convergence might result in a rate of convergence that is higher than the order of accuracy [3]. The rate of convergence of the scheme in the gradually stretched grid can be increased or decreased by adjusting the grid stretching factor, as is demonstrated in [18]. The super-convergence is not simply a grid phenomenon; in some circumstances, lower-order boundary treatment also leads to super-convergence [19]. Although the super-convergence phenomenon is beneficial, we are unaware of any prior numerical analysis that can be used to predict super-convergence phenomena for a given problem. Some researchers claim that when a non-uniform grid is adopted, the order of accuracy or rate of convergence of conservative discretization is unaffected [7–17]. Others claim that when a non-uniform grid is chosen, the order of accuracy in conservative discretization is reduced [6, 20–27]. The degradation of the order of accuracy also depends on the nature of the equation. For example, hyperbolic equations are considerably more sensitive to the grid quality than elliptic ones [23].

Poor convergence or divergence in the numerical solution obtained by CFD software is commonly attributed to the quality of the computational grid. It is quite difficult [28] to derive a comprehensive proof of discretization error and the rate of convergence on an FVM-based unstructured grid. On a Cartesian grid, an FVM is simplified to a conservative finite difference method (CFDM) [29]. It is relatively easier to investigate the discretization error and rate of convergence of a conservative FDM compared to an FVM on an unstructured grid. The error associated with the unstructured FVM is significantly greater than that associated with the FVM on the Cartesian grid because of interpolation, skewness, non-orthogonality, Jacobian transformation, and other factors. The theoretical order of accuracy and the rate of convergence of the higher-order CFDM on an arbitrarily varying non-uniform grid are studied in some basic test cases. We employed a symbolic computational tool in MATLAB software to do this because the theoretical proof for the order of accuracy by expanding the Taylor series is exhaustive for an arbitrarily varying non-uniform grid.

In this work, we use a conservative framework used in the WENO schemes [5] that we denote here as CFDM. The non-uniform version of CFDM is denoted as NCFDM. In the same way, NFDM stands for a non-uniform finite difference technique. The FVM is commonly used in most fluid dynamics simulation software packages. These programs require smoothly varying grids to get better convergence. When an arbitrarily varying non-uniform grid is employed, it may show divergence or poor convergence rate. We investigate the order of accuracy and rate of convergence of conservative discretization on several test cases implemented on different grid configurations. The performance of NCFDM and NFDM on a uniform grid (U-grid), a non-uniform grid

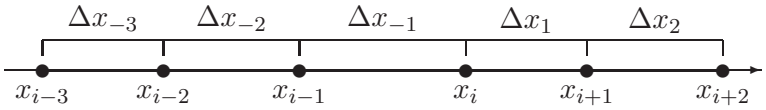

Fig. 1: Arbitrary varying non-uniform grid

(NU-grid), and a grid whose mesh widths in arithmetic progression (AP-grid) were investigated for the test cases of derivative calculation (i.e., of pointwise values of the derivative of a given function), the linear convection equation (LCE), the linear convection-diffusion equation (LCDE), the lid-driven cavity problem, and the Taylor-Green vortex problem.

For a smooth solution, we need higher-order schemes to attain a high rate of convergence. The accuracy of the solution depends not only on the schemes we used but also on the grid we have chosen. Several articles formulate numerical algorithms for non-uniform grids [30–36]. The higher-order finite difference scheme for a non-uniform grid is presented in [10, 30, 31] and compact difference schemes are presented in [32–34]. In the above literature, a linear transformation is deployed in the grid generation, but in the present work, the grid is completely random and non-overlapping. We have derived a generalized formula for derivative calculation without any mesh distribution function, so the stencil size is much bigger than the above-mentioned works.

The paper is organized as follows. A brief introduction to the method and procedure to develop conservative and non-conservative methods on uniform and non-uniform grids are presented in section 2. There is no explicit NCFDM on an arbitrarily varying grid available in the literature. So, we derive a formula to calculate the theoretical order of accuracy. This may be the first work to present the explicit formulation of the CFDM on an arbitrarily varying non-uniform grid and study the theoretical order of accuracy. The performance of the NFDM and NCFDM on the derivative calculation, linear convection equation, convection-diffusion equation, lid-driven cavity, and Taylor-Green vortex problem using non-uniform, AP-grid, and the uniform grid are presented in section 3. Conclusions are collected in section 4.

2 Schemes used in this work

The procedure to derive the conservative discretization on the uniform and non-uniform grids is described in this section. To derive a higher-order conservative scheme on a uniform mesh, we adopt the techniques utilized by Shu and Osher [5]. Here, the method used for conservative discretization is extended to arbitrary shifting non-uniform grids.

2.1 Finite difference method on a non-uniform grid

We derive a four-point finite difference method on the stencil $\{x_{i-2}, x_{i-1}, x_i, x_{i+1}\}$ on a non-uniform grid. To this end a polynomial-based approach is employed [37]. See Figure 1 for the mesh widths and nomenclature. To maintain uniformity in the order of accuracy of various schemes when developing FD schemes, the grid points x_{i-3} and x_{i+2} are not used, but they are used in the conservative finite difference framework.

Assume now that we seek to calculate an approximate value of the derivative at $x = 0$ of a sufficiently smooth function $u = u(x)$ when only the values $u(x_{i-2}), \dots, u(x_{i+1})$ are known, and we therefore need to take the derivative of the unique interpolating cubic polynomial, written in monomial form as $p(x) = a_0 + a_1 x + a_2 x^2 + a_3 x^3$. For ease of notation, we assume that $x_i = 0$. The derivative of $p(x)$ at $x = 0$ is

$$\left.\frac{\mathrm{d}u}{\mathrm{d}x}\right|_{x=0} \approx \left.\frac{\mathrm{d}p}{\mathrm{d}x}\right|_{x=0} = a_1, \tag{2.1}$$

and the coefficients $a_0, \dots, a_3$ of p are identified from the requirements

$$\begin{aligned} &p(x_{i-2}) = u_{i-2} := u(-\Delta x_{-2} - \Delta x_{-1}), \quad p(x_{i-1}) = u_{i-1} := u(-\Delta x_{-1}), \\ &p(x_i) = u_i := u(0), \quad p(x_{i+1}) = u_{i+1} := u(\Delta x_1). \end{aligned} \tag{2.2}$$

Solving the system defined by (2.2), namely

$$\begin{bmatrix} 1 & -(\Delta x_{-2} + \Delta x_{-1}) & (\Delta x_{-2} + \Delta x_{-1})^2 & -(\Delta x_{-2} + \Delta x_{-1})^3 \\ 1 & -\Delta x_{-1} & \Delta x_{-1}^2 & -\Delta x_{-1}^3 \\ 1 & 0 & 0 & 0 \\ 1 & \Delta x_1 & \Delta x_1^2 & \Delta x_1^3 \end{bmatrix} \begin{pmatrix} a_0 \\ a_1 \\ a_2 \\ a_3 \end{pmatrix} = \begin{pmatrix} u_{i-2} \\ u_{i-1} \\ u_i \\ u_{i+1} \end{pmatrix},$$

for $a_0, \dots, a_3$ in terms of $u_{i-2}, \dots, u_{i+1}$ gives, by Cramer's rule, $a_0 = u_i$, $a_1 = n_1/d_1$, $a_2 = n_2/d_1$, and $a_3 = n_3/d_1$, where

$$\begin{aligned} n_1 = {} & (u_i - u_{i-1})(\Delta x_1^2 \Delta x_{-2}^3 + \Delta x_1^3 \Delta x_{-2}^2 + 2\Delta x_1^3 \Delta x_{-1} \Delta x_{-2} \\ & + 3\Delta x_1^2 \Delta x_{-1} \Delta x_{-2}^2 + 3\Delta x_1^2 \Delta x_{-1}^2 \Delta x_{-2}) \\ & + (u_{i+1} - u_i)(\Delta x_{-1}^2 \Delta x_{-2}^3 + 2\Delta x_{-1}^3 \Delta x_{-2}^2 + \Delta x_{-1}^4 \Delta x_{-2}) \\ & + (u_{i-2} - u_{i-1})(\Delta x_1^2 \Delta x_{-1}^3 + \Delta x_1^3 \Delta x_{-1}^2), \\ d_1 = {} & \Delta x_1 \Delta x_{-1} \Delta x_{-2} (\Delta x_1 + \Delta x_{-1})(\Delta x_{-1} + \Delta x_{-2})(\Delta x_1 + \Delta x_{-1} + \Delta x_{-2}). \end{aligned}$$

(Since we are only interested in a_1, the expressions for n_2 and n_3 are not written out here.)

Theorem 1. *The order of approximation in (2.1) is three, that is if we assume that $\Delta x_i < h$ for all i, then*

$$\left.\frac{\mathrm{d}u}{\mathrm{d}x}\right|_{x=x_i} = \left.\frac{\mathrm{d}p}{\mathrm{d}x}\right|_{x=x_i} + \mathcal{O}(h^3) = a_1 + \mathcal{O}(h^3) \quad \text{as } h \to 0. \tag{2.3}$$

Proof. To make the proof as short as possible, let us set

$$r := \Delta x_{-2}, \quad s := \Delta x_{-1}, \quad t := \Delta x_1. \tag{2.4}$$

We then get

$$\begin{aligned} n_1 &= \lambda_1 \frac{u_i - u_{i-1}}{s} + \lambda_2 \frac{u_{i+1} - u_i}{t} + \lambda_3 \frac{u_{i-1} - u_{i-2}}{r} \\ &= \lambda_1 \frac{u_i - u_{i-1}}{s} + \lambda_2 \frac{u_{i+1} - u_i}{t} + \lambda_3 \left(-\frac{s}{r} \frac{u_i - u_{i-1}}{s} + \frac{r+s}{r} \frac{u_i - u_{i-2}}{r+s} \right) \\ &= \left(\lambda_1 - \frac{s}{r} \lambda_3 \right) \frac{u_i - u_{i-1}}{s} + \lambda_2 \frac{u_{i+1} - u_i}{t} + \frac{r+s}{r} \lambda_3 \frac{u_i - u_{i-2}}{r+s} \end{aligned} \tag{2.5}$$

where

$$\lambda_1 = rst^2(r^2 + rt + 2st + 3rs + 3s^2), \quad \lambda_2 = rs^2t(r+s)^2, \quad \lambda_3 = -rs^2t^2(s+t),$$
$$d_1 = rst(s+t)(r+s)(r+s+t).$$

We now wish to apply the Taylor expansions

$$\begin{aligned} \frac{u_i - u_{i-1}}{s} &= \frac{\mathrm{d}u}{\mathrm{d}x}(x_i) - \frac{s}{2}\frac{\mathrm{d}^2u}{\mathrm{d}x^2}(x_i) + \frac{s^2}{6}\frac{\mathrm{d}^3u}{\mathrm{d}x^3}(x_i) - \frac{s^3}{24}\frac{\mathrm{d}^4u}{\mathrm{d}x^4}(x_i) + \mathcal{O}(s^4), \\ \frac{u_{i+1} - u_i}{t} &= \frac{\mathrm{d}u}{\mathrm{d}x}(x_i) + \frac{t}{2}\frac{\mathrm{d}^2u}{\mathrm{d}x^2}(x_i) + \frac{t^2}{6}\frac{\mathrm{d}^3u}{\mathrm{d}x^3}(x_i) + \frac{t^3}{24}\frac{\mathrm{d}^4u}{\mathrm{d}x^4}(x_i) + \mathcal{O}(t^4), \\ \frac{u_i - u_{i-2}}{r+s} &= \frac{\mathrm{d}u}{\mathrm{d}x}(x_i) - \frac{r+s}{2}\frac{\mathrm{d}^2u}{\mathrm{d}x^2}(x_i) + \frac{(r+s)^2}{6}\frac{\mathrm{d}^3u}{\mathrm{d}x^3}(x_i) - \frac{(r+s)^3}{24}\frac{\mathrm{d}^4u}{\mathrm{d}x^4}(x_i) \\ &\quad + \mathcal{O}(r^4 + s^4) \end{aligned}$$

as $r, s, t \to 0$. Inserting these expressions into (2.5), taking into account that

$$\begin{aligned} \left(\lambda_1 - \frac{s}{r}\lambda_3 \right) + \lambda_2 + \frac{r+s}{r}\lambda_3 &= \lambda_1 + \lambda_2 + \lambda_3 = d_1, \\ -\frac{s}{2}\left(\lambda_1 - \frac{s}{r}\lambda_3 \right) + \frac{t}{2}\lambda_2 - \frac{(r+s)^2}{2r}\lambda_3 &= 0, \\ \frac{s^2}{6}\left(\lambda_1 - \frac{s}{r}\lambda_3 \right) + \frac{t^2}{6}\lambda_2 - \frac{(r+s)^3}{6r}\lambda_3 &= 0, \\ -\frac{s^3}{24}\left(\lambda_1 - \frac{s}{r}\lambda_3 \right) + \frac{t^3}{24}\lambda_2 - \frac{(r+s)^4}{24r}\lambda_3 &= \\ \frac{rs^2t^2}{24}(r+s)^2(s+t)(r+s+t) &= \frac{st(r+s)}{24}d_1, \end{aligned} \tag{2.6}$$

and reverting to the previous notation, we get

$$a_1 = \frac{n_1}{d_1} = \frac{\mathrm{d}u}{\mathrm{d}x}(x_i) + \frac{1}{24}\Delta x_1 \Delta x_{-1}(\Delta x_{-1} + \Delta x_{-2})\frac{\mathrm{d}^4u}{\mathrm{d}x^4}(x_i + \vartheta h), \quad 0 \le \vartheta \le 1.$$

This proves (2.3) if we consider that $\Delta x_1 \Delta x_{-1}(\Delta x_{-1} + \Delta x_{-2}) = \mathcal{O}(h^3)$ as $h \to 0$. □

2.2 Conservative finite difference method (CFDM) on the uniform grids

Here, we shall discuss the approach widely used in essentially non-oscillatory (ENO) schemes [38] and WENO schemes [39, 40]. Conservative discretizations are based on cell averages. We define the cell average of u on the cell $[x_{i-1/2}, x_{i+1/2}]$ as

$$\bar{u}(x) := \frac{1}{\Delta x}\int_{x-\Delta x/2}^{x+\Delta x/2} u(\xi)\,\mathrm{d}\xi. \tag{2.7}$$

The cell averages associated with $x = x_{i-1}, x_i, x_{i+1}$ are

$$\bar{u}_{i+k} := \bar{u}(x_{i+k}) = \frac{1}{\Delta x}\int_{x_{i+k-1/2}}^{x_{i+k+1/2}} u(\xi)\,\mathrm{d}\xi, \quad k = -1, 0, 1.$$

To derive a third-order formulation, we assume that $u = p$ is a quadratic polynomial $p(\xi) = a + b\xi + c\xi^2$. Substituting this polynomial into (2.7) and integrating gives $\bar{p}(x) = a + bx + c(x^2 + \Delta x^2/12)$. Suppose now that $\bar{u}_{i-1}$, $\bar{u}_i$ and $\bar{u}_{i+1}$ are given cell averages of an arbitrary function u and we seek the coefficients a, b and c of the quadratic polynomial p that produces the same cell averages. To this end, we solve the equations $\bar{p}(x_{i+k}) = \bar{u}_{i+k}$, $k = -1, 0, 1$, for a, b and c, which yields

$$\begin{aligned}
a &= a(\bar{u}_{i-1}, \bar{u}_i, \bar{u}_{i+1}) = \frac{1}{2}\bar{u}_{i+1} - \bar{u}_i + \frac{1}{2}\bar{u}_{i-1},\\
b &= b(\bar{u}_{i-1}, \bar{u}_i, \bar{u}_{i+1}) = \frac{1}{2}\bar{u}_{i+1} - \frac{1}{2}\bar{u}_{i-1},\\
c &= c(\bar{u}_{i-1}, \bar{u}_i, \bar{u}_{i+1}) = -\frac{1}{24}\bar{u}_{i+1} + \frac{13}{12}\bar{u}_i - \frac{1}{24}\bar{u}_{i-1}.
\end{aligned}$$

After computing a, b and c, we obtain the cell-interface values

$$p_{i+1/2} = a\left(\frac{\Delta x}{2}\right)^2 + b\frac{\Delta x}{2} + c = -\frac{1}{6}\bar{u}_{i-1} + \frac{5}{6}\bar{u}_i + \frac{1}{3}\bar{u}_{i+1}. \tag{2.8}$$

To calculate left cell-interface values, we now employ

$$a = a(\bar{u}_{i-2}, \bar{u}_{i-1}, \bar{u}_i) = \frac{1}{2}\bar{u}_{i-2} - \bar{u}_{i-1} + \frac{1}{2}\bar{u}_i, \tag{2.9}$$

$$b = b(\bar{u}_{i-2}, \bar{u}_{i-1}, \bar{u}_i) = \frac{1}{2}\bar{u}_{i-2} - 2\bar{u}_{i-1} + \frac{3}{2}\bar{u}_i, \tag{2.10}$$

$$c = c(\bar{u}_{i-2}, \bar{u}_{i-1}, \bar{u}_i) = -\frac{1}{24}\bar{u}_{i-2} + \frac{1}{12}\bar{u}_{i-1} + \frac{23}{24}\bar{u}_i \tag{2.11}$$

to obtain

$$p_{i-1/2} = a\left(-\frac{\Delta x}{2}\right)^2 + b\left(-\frac{\Delta x}{2}\right) + c = -\frac{1}{6}\bar{u}_{i-2} + \frac{5}{6}\bar{u}_{i-1} + \frac{1}{3}\bar{u}_i. \tag{2.12}$$

The coefficients of (2.8) and (2.12) are the same but the grid index is shifted by one. This so-called *index shifting property* [18, 41] is required to achieve higher-order accuracy in the conservative discretization, which is only possible on a uniform grid and is in general impossible on an arbitrarily varying non-uniform grid. The derivative of u can be approximated in the conservative framework via

$$p'(x_i) = \frac{u_{i+1/2} - u_{i-1/2}}{\Delta x} \tag{2.13}$$

(this formula is exact since p is a quadratic polynomial). Substituting (2.8) and (2.12) into (2.13) gives

$$\frac{\mathrm{d}\bar{u}}{\mathrm{d}x}(x_i) = p'(x_i) + \mathcal{O}(\Delta x^3) = \frac{1}{6\Delta x}\left(2\bar{u}_{i+1} + 3\bar{u}_i - 6\bar{u}_{i-1} + \bar{u}_{i-2}\right) + \mathcal{O}(\Delta x^3). \tag{2.14}$$

Equation (2.14) is a third-order accurate conservative finite difference formulation which is equivalent to a standard finite difference scheme.

2.3 Higher-order conservative discretization on an arbitrary varying non-uniform grid (NCFDM)

An explicit formula for conservative discretization on an arbitrarily varying non-uniform grid is not available, so we extend the method for the uniform mesh of Section 2.2 to a non-uniform grid. The cell averages are now defined by

$$\begin{aligned}
\bar{u}_{i-2} &= \frac{2}{\Delta x_{-2} + \Delta x_{-3}} \int_{x_i - (\Delta x_{-1} + \Delta x_{-2} + \Delta x_{-3}/2)}^{x_i - (\Delta x_{-1} + \Delta x_{-2}/2)} u(\xi)\,\mathrm{d}\xi, \\
\bar{u}_{i-1} &= \frac{2}{\Delta x_{-1} + \Delta x_{-2}} \int_{x_i - (\Delta x_{-1} + \Delta x_{-2}/2)}^{x_i - \Delta x_{-1}/2} u(\xi)\,\mathrm{d}\xi, \\
\bar{u}_{i} &= \frac{2}{\Delta x_{-1} + \Delta x_{1}} \int_{x_i - \Delta x_{-1}/2}^{x_i + \Delta x_{1}/2} u(\xi)\,\mathrm{d}\xi, \\
\bar{u}_{i+1} &= \frac{2}{\Delta x_{1} + \Delta x_{2}} \int_{x_i + \Delta x_{1}/2}^{x_i + (\Delta x_{1} + \Delta x_{2}/2)} u(\xi)\,\mathrm{d}\xi.
\end{aligned} \tag{2.15}$$

Substituting the polynomial $p(\xi) = a + b\xi + c\xi^2$ into (2.15), solving for a, b and c in terms of given cell averages $\bar{u}_{i-2}, \ldots, \bar{u}_{i+1}$, and using these values of a, b and c to calculate cell-interface values, we obtain

$$p_{i-1/2} = a\left(-\frac{\Delta x_{-1}}{2}\right)^2 + b\left(-\frac{\Delta x_{-1}}{2}\right) + c, \quad p_{i+1/2} = a\left(\frac{\Delta x_{1}}{2}\right)^2 + b\left(\frac{\Delta x_{1}}{2}\right) + c,$$

where by using Cramer's rule in a way similar to the proof of Theorem 1, we get $a = N_a/D_d$, $b = N_b/D_d$ and $c = N_c/D_d$ with

$$N_a = 12(\bar{u}_{i+1}\Delta x_1 - \bar{u}_i\Delta x_2 - 3\bar{u}_i\Delta x_1 - 3\bar{u}_i\Delta x_{-1} - \bar{u}_i\Delta x_{-2} + 2\bar{u}_{i+1}\Delta x_{-1}$$

$$
\begin{aligned}
&+ 2\bar{u}_{i-1}\Delta x_1 + \bar{u}_{i+1}\Delta x_{-2} + \bar{u}_{i-1}\Delta x_2 + \bar{u}_{i-1}\Delta x_{-1}),\\
D_d &= (\Delta x_1 + 2\Delta x_{-1} + \Delta x_{-2})(4\Delta x_1^2 + 4\Delta x_1\Delta x_2 + 6\Delta x_1\Delta x_{-1} + 2\Delta x_{-2}\Delta x_1\\
&+ \Delta x_2^2 + 3\Delta x_2\Delta x_{-1} + \Delta x_{-2}\Delta x_2 + 2\Delta x_{-1}^2 + \Delta x_{-2}\Delta x_{-1}),\\
N_b &= 4(7\bar{u}_i\Delta x_1^2 + \bar{u}_i\Delta x_2^2 - \bar{u}_{i+1}\Delta x_1^2 - 7\bar{u}_i\Delta x_{-1}^2 - \bar{u}_i\Delta x_{-2}^2 + 6\bar{u}_{i+1}\Delta x_{-1}^2\\
&- 6\bar{u}_{i-1}\Delta x_1^2 + \bar{u}_{i+1}\Delta x_{-2}^2 - \bar{u}_{i-1}\Delta x_2^2 + \bar{u}_{i-1}\Delta x_{-1}^2 + 5\bar{u}_i\Delta x_1\Delta x_2\\
&+ \bar{u}_{i+1}\Delta x_1\Delta x_{-1} - 5\bar{u}_{i-1}\Delta x_1\Delta x_2 - 5\bar{u}_i\Delta x_{-1}\Delta x_{-2} - \bar{u}_{i-1}\Delta x_1\Delta x_{-1}\\
&+ 5\bar{u}_{i+1}\Delta x_{-1}\Delta x_{-2}),\\
N_c &= 4\bar{u}_{i+1}\Delta x_{-1}^3 + 4\bar{u}_{i-1}\Delta x_1^3 + 21\bar{u}_i\Delta x_1\Delta x_{-1}^2 + 21\bar{u}_i\Delta x_1^2\Delta x_{-1} + 3\bar{u}_i\Delta x_1\Delta x_{-2}^2\\
&+ 7\bar{u}_i\Delta x_2\Delta x_{-1}^2 + 7\bar{u}_i\Delta x_1^2\Delta x_{-2} + 3\bar{u}_i\Delta x_2^2\Delta x_{-1} - 4\bar{u}_{i+1}\Delta x_1\Delta x_{-1}^2\\
&- 3\bar{u}_{i+1}\Delta x_1^2\Delta x_{-1} + \bar{u}_i\Delta x_2\Delta x_{-2}^2 + \bar{u}_i\Delta x_2^2\Delta x_{-2} - \bar{u}_{i+1}\Delta x_1\Delta x_{-2}^2\\
&- \bar{u}_{i+1}\Delta x_1^2\Delta x_{-2} + \bar{u}_{i-1}\Delta x_1\Delta x_2^2 + 4\bar{u}_{i-1}\Delta x_1^2\Delta x_2 - 3\bar{u}_{i-1}\Delta x_1\Delta x_{-1}^2\\
&- 4\bar{u}_{i-1}\Delta x_1^2\Delta x_{-1} + \bar{u}_{i+1}\Delta x_{-1}\Delta x_{-2}^2 + 4\bar{u}_{i+1}\Delta x_{-1}^2\Delta x_{-2}\\
&- \bar{u}_{i-1}\Delta x_2\Delta x_{-1}^2 - \bar{u}_{i-1}\Delta x_2^2\Delta x_{-1} + 15\bar{u}_i\Delta x_1\Delta x_2\Delta x_{-1}\\
&+ 5\bar{u}_i\Delta x_1\Delta x_2\Delta x_{-2} + 15\bar{u}_i\Delta x_1\Delta x_{-1}\Delta x_{-2} + 5\bar{u}_i\Delta x_2\Delta x_{-1}\Delta x_{-2}\\
&- 4\bar{u}_1\Delta x_1\Delta x_{-1}\Delta x_{-2} - 4\bar{u}_{-1}\Delta x_1\Delta x_2\Delta x_{-1}
\end{aligned}
$$

Finally, the derivative of p at $x = x_i$ can be calculated using

$$
\frac{\mathrm{d}\bar{p}}{\mathrm{d}x} = 2\frac{p_{i+1/2} - p_{i-1/2}}{\Delta x_{-1} + \Delta x_1} = \frac{2}{\Delta x_{-1} + \Delta x_1}\left(\frac{N_1}{D_1} - \frac{N_2}{D_2}\right), \tag{2.16}
$$

where

$$
\begin{aligned}
N_1 &= 5\bar{u}_i\Delta x_1^3 + \bar{u}_{i+1}\Delta x_1^3 + 4\bar{u}_{i+1}\Delta x_{-1}^3 - 2\bar{u}_{i-1}\Delta x_1^3 + 2\bar{u}_i\Delta x_1\Delta x_2^2 + 7\bar{u}_i\Delta x_1^2\Delta x_2\\
&+ 7\bar{u}_i\Delta x_1\Delta x_{-1}^2 + 12\bar{u}_i\Delta x_1^2\Delta x_{-1} + \bar{u}_i\Delta x_1\Delta x_{-2}^2 + 7\bar{u}_i\Delta x_2\Delta x_{-1}^2\\
&+ 3\bar{u}_i\Delta x_2^2\Delta x_{-1} + 8\bar{u}_{i+1}\Delta x_1\Delta x_{-1}^2 + 5\bar{u}_{i+1}\Delta x_1^2\Delta x_{-1} + \bar{u}_i\Delta x_2\Delta x_{-2}^2\\
&+ \bar{u}_{i+1}\Delta x_1\Delta x_{-2}^2 + 2\bar{u}_{i+1}\Delta x_1^2\Delta x_{-2} - \bar{u}_{i-1}\Delta x_1\Delta x_2^2 - 3\bar{u}_{i-1}\Delta x_1^2\Delta x_2\\
&- 3\bar{u}_{i-1}\Delta x_1^2\Delta x_{-1} + \bar{u}_{i+1}\Delta x_{-1}\Delta x_{-2}^2 + 4\bar{u}_{i+1}\Delta x_{-1}^2\Delta x_{-2} - \bar{u}_{i-1}\Delta x_1\Delta x_{-1}^2\\
&- \bar{u}_{i-1}\Delta x_2^2\Delta x_{-1} + 15\bar{u}_i\Delta x_1\Delta x_2\Delta x_{-1} - 4\bar{u}_{i-1}\Delta x_1\Delta x_2\Delta x_{-1} + \bar{u}_i\Delta x_2^2\Delta x_{-2}\\
&+ 5\bar{u}_i\Delta x_1\Delta x_{-1}\Delta x_{-2} + 5\bar{u}_i\Delta x_2\Delta x_{-1}\Delta x_{-2} + 4\bar{u}_i\Delta x_1^2\Delta x_{-2} - \bar{u}_{i-1}\Delta x_2\Delta x_{-1}^2\\
&- \bar{u}_{i-1}\Delta x_2\Delta x_{-1}^2 + 5\bar{u}_i\Delta x_1\Delta x_2\Delta x_{-2} + 6\bar{u}_{i+1}\Delta x_1\Delta x_{-1}\Delta x_{-2},\\
D_1 &= (2\Delta x_1 + \Delta x_2 + \Delta x_{-1})(\Delta x_1 + 2\Delta x_{-1} + \Delta x_{-2})\\
&\times (2\Delta x_1 + \Delta x_2 + 2\Delta x_{-1} + \Delta x_{-2}),\\
N_2 &= \bar{u}_i\Delta x_{-1}^3 + 4\bar{u}_i\Delta x_{-2}^3 + 5\bar{u}_{i-1}\Delta x_{-1}^3 - 2\bar{u}_{i-2}\Delta x_{-1}^3 + 8\bar{u}_i\Delta x_{-1}\Delta x_{-2}^2\\
&+ 7\bar{u}_{i-1}\Delta x_1\Delta x_{-1}^2 + 2\bar{u}_{i-1}\Delta x_1^2\Delta x_{-1} + \bar{u}_i\Delta x_{-1}\Delta x_{-3}^2 + 2\bar{u}_i\Delta x_{-1}^2\Delta x_{-3}\\
&+ 7\bar{u}_{i-1}\Delta x_1\Delta x_{-2}^2 + 3\bar{u}_{i-1}\Delta x_1^2\Delta x_{-2} - 3\bar{u}_{i-2}\Delta x_1\Delta x_{-1}^2 - \bar{u}_{i-2}\Delta x_1^2\Delta x_{-1}\\
&+ 4\bar{u}_i\Delta x_{-2}^2\Delta x_{-3} + \bar{u}_{i-1}\Delta x_1\Delta x_{-3}^2 + \bar{u}_{i-1}\Delta x_1^2\Delta x_{-3} - \bar{u}_{i-2}\Delta x_1\Delta x_{-2}^2
\end{aligned}
$$

$$
\begin{aligned}
&+ 7\bar{u}_{i-1}\Delta x_{-1}\Delta x_{-2}^2 + 12\bar{u}_{i-1}\Delta x_{-1}^2\Delta x_{-2} + \bar{u}_{i-1}\Delta x_{-1}\Delta x_{-3}^2 \\
&- \bar{u}_{i-2}\Delta x_{-1}\Delta x_{-2}^2 - 3\bar{u}_{i-2}\Delta x_{-1}^2\Delta x_{-2} + 15\bar{u}_{i-1}\Delta x_1\Delta x_{-1}\Delta x_{-2} \\
&+ 5\bar{u}_{i-1}\Delta x_1\Delta x_{-1}\Delta x_{-3} - 4\bar{u}_{i-2}\Delta x_1\Delta x_{-1}\Delta x_{-2} + \bar{u}_i\Delta x_{-2}\Delta x_{-3}^2 \\
&+ 5\bar{u}_{i-1}\Delta x_1\Delta x_{-2}\Delta x_{-3} + 5\bar{u}_{i-1}\Delta x_{-1}\Delta x_{-2}\Delta x_{-3} + 5\bar{u}_i\Delta x_{-1}^2\Delta x_{-2} \\
&- \bar{u}_{i-2}\Delta x_1^2\Delta x_{-2} + 6\bar{u}_i\Delta x_{-1}\Delta x_{-2}\Delta x_{-3} + 4\bar{u}_{i-1}\Delta x_{-1}^2\Delta x_{-3}, \\
D_2 = &(\Delta x_1 + 2\Delta x_{-1} + \Delta x_{-2})(\Delta x_{-1} + 2\Delta x_{-2} + \Delta x_{-3}) \\
&\times (\Delta x_1 + 2\Delta x_{-1} + 2\Delta x_{-2} + \Delta x_{-3}).
\end{aligned}
$$

Here the quantities $\bar{u}_{i-2}, \ldots, \bar{u}_{i+1}$ are given by

$$
\bar{u}_{i-2} = u(-\Delta x_{-1} - \Delta x_{-2}), \quad \bar{u}_{i-1} = u(-\Delta x_{-1}), \quad \bar{u}_i = u(0), \quad \bar{u}_{i+1} = u(\Delta x_1).
$$

Theorem 2. *Only in certain exceptional cases of grid spacing the derivative of $\bar{p}(x)$ at $x = x_i$, given by (2.16), is a first-order accurate approximation to $\mathrm{d}\bar{u}/\mathrm{d}x|_{x=x_i}$.*

Proof. The Taylor expansion of $\bar{u}$ at x_i up to the first derivative term is

$$
\bar{u}(x_i + \tau) = \bar{u}(x_i) + \tau\frac{\mathrm{d}\bar{u}}{\mathrm{d}x}(x_i) + \mathcal{O}(\tau) \quad \text{as } \tau \to 0. \tag{2.17}
$$

The computational molecules n_1, n_2, d_1 and d_2 in (2.16) involve $\bar{u}_{i-2}$, $\bar{u}_{i-1}$, $\bar{u}_i$, and $\bar{u}_{i+1}$. Thus, the Taylor expansions of each term give

$$
\begin{aligned}
\bar{u}_{i-2} &= \bar{u}(x_i) + (-\Delta x_{-1} - \Delta x_{-2})\,\frac{\mathrm{d}\bar{u}}{\mathrm{d}x}(x_i) + \text{h.o.t.}, \\
\bar{u}_{i-1} &= \bar{u}(x_i) + (-\Delta x_{-1})\,\frac{\mathrm{d}\bar{u}}{\mathrm{d}x}(x_i) + \text{h.o.t.}, \\
\bar{u}_i &= \bar{u}(x_i), \\
\bar{u}_{i+1} &= \bar{u}(x_i) + (\Delta x_1)\,\frac{\mathrm{d}\bar{u}}{\mathrm{d}x}(x_i) + \text{h.o.t.},
\end{aligned} \tag{2.18}
$$

where h.o.t. denotes higher-order terms in the Taylor expansion. Substituting (2.18) into (2.16) and expanding each term using the Taylor series gives

$$
\left.\frac{\mathrm{d}\bar{p}}{\mathrm{d}x}\right|_{x=x_i} = \frac{\mathrm{d}\bar{u}}{\mathrm{d}x}(x_i)\frac{n_a}{d_a}, \tag{2.19}
$$

where

$$
\begin{aligned}
n_a = &2(\Delta x_1^4\Delta x_{-1} + 2\Delta x_1^4\Delta x_{-2} + \Delta x_1^4\Delta x_{-3} + 12\Delta x_1^3\Delta x_{-1}^2 \\
&+ 24\Delta x_1^3\Delta x_{-1}\Delta x_{-2} + 13\Delta x_1^3\Delta x_{-1}\Delta x_{-3} + 4\Delta x_1^3\Delta x_{-2}^2 + 6\Delta x_1^3\Delta x_{-2}\Delta x_{-3} \\
&+ \Delta x_1^3\Delta x_{-3}^2 + 7\Delta x_1^2\Delta x_2\Delta x_{-1}^2 + 10\Delta x_1^2\Delta x_2\Delta x_{-1}\Delta x_{-2} + 7\Delta x_1^2\Delta x_2\Delta x_{-1}\Delta x_{-3} \\
&- 4\Delta x_1^2\Delta x_2\Delta x_{-2}^2 + 35\Delta x_1^2\Delta x_{-1}^3 + 90\Delta x_1^2\Delta x_{-1}^2\Delta x_{-2} + 45\Delta x_1^2\Delta x_{-1}^2\Delta x_{-3}
\end{aligned}
$$

$$
\begin{aligned}
&+ 53\Delta x_1^2\Delta x_{-1}\Delta x_{-2}^2 + 56\Delta x_1^2\Delta x_{-1}\Delta x_{-2}\Delta x_{-3} + 10\Delta x_1^2\Delta x_{-1}\Delta x_{-3}^2 \\
&+ 4\Delta x_1^2\Delta x_{-2}^3 + 9\Delta x_1^2\Delta x_{-2}^2\Delta x_{-3} + 2\Delta x_1^2\Delta x_{-2}\Delta x_{-3}^2 + 2\Delta x_1\Delta x_2^2\Delta x_{-1}^2 \\
&+ 3\Delta x_1\Delta x_2^2\Delta x_{-1}\Delta x_{-2} + 2\Delta x_1\Delta x_2^2\Delta x_{-1}\Delta x_{-3} - \Delta x_1\Delta x_2^2\Delta x_{-2}^2 \\
&+ 22\Delta x_1\Delta x_2\Delta x_{-1}^3 + 52\Delta x_1\Delta x_2\Delta x_{-1}^2\Delta x_{-2} + 29\Delta x_1\Delta x_2\Delta x_{-1}^2\Delta x_{-3} \\
&+ 22\Delta x_1\Delta x_2\Delta x_{-1}\Delta x_{-2}^2 + 33\Delta x_1\Delta x_2\Delta x_{-1}\Delta x_{-2}\Delta x_{-3} + 7\Delta x_1\Delta x_2\Delta x_{-1}\Delta x_{-3}^2 \\
&- 5\Delta x_1\Delta x_2\Delta x_{-2}^3 + 30\Delta x_1\Delta x_{-1}^4 + 89\Delta x_1\Delta x_{-1}^3\Delta x_{-2} + 41\Delta x_1\Delta x_{-1}^3\Delta x_{-3} \\
&+ 77\Delta x_1\Delta x_{-1}^2\Delta x_{-2}^2 + 71\Delta x_1\Delta x_{-1}^2\Delta x_{-2}\Delta x_{-3} + 11\Delta x_1\Delta x_{-1}^2\Delta x_{-3}^2 \\
&+ 21\Delta x_1\Delta x_{-1}\Delta x_{-2}^3 + 29\Delta x_1\Delta x_{-1}\Delta x_{-2}^2\Delta x_{-3} \\
&+ 6\Delta x_1\Delta x_{-1}\Delta x_{-2}\Delta x_{-3}^2 + 2\Delta x_1\Delta x_{-2}^4 + 4\Delta x_1\Delta x_{-2}^3\Delta x_{-3} + \Delta x_1\Delta x_{-2}^2\Delta x_{-3}^2 \\
&+ 5\Delta x_2^2\Delta x_{-1}^3 + 13\Delta x_2^2\Delta x_{-1}^2\Delta x_{-2} + 17\Delta x_{-1}^4\Delta x_{-2} + 8\Delta x_{-1}^4\Delta x_{-3} \\
&+ 7\Delta x_2^2\Delta x_{-1}^2\Delta x_{-3} + 7\Delta x_2^2\Delta x_{-1}\Delta x_{-2}^2 + 9\Delta x_2^2\Delta x_{-1}\Delta x_{-2}\Delta x_{-3} \\
&+ 2\Delta x_2^2\Delta x_{-1}\Delta x_{-3}^2 - \Delta x_2^2\Delta x_{-2}^3 + 11\Delta x_2\Delta x_{-1}^4 + 30\Delta x_2\Delta x_{-1}^3\Delta x_{-2} \\
&+ 15\Delta x_2\Delta x_{-1}^3\Delta x_{-3} + 20\Delta x_2\Delta x_{-1}^2\Delta x_{-2}^2 + 23\Delta x_2\Delta x_{-1}^2\Delta x_{-2}\Delta x_{-3} \\
&+ 4\Delta x_2\Delta x_{-1}^2\Delta x_{-3}^2 + 5\Delta x_2\Delta x_{-1}\Delta x_{-2}^2\Delta x_{-3} + \Delta x_2\Delta x_{-1}\Delta x_{-2}\Delta x_{-3}^2 \\
&+ 13\Delta x_{-1}^3\Delta x_{-2}^2 + 14\Delta x_{-1}^3\Delta x_{-2}\Delta x_{-3} + 2\Delta x_{-1}^3\Delta x_{-3}^2 + \Delta x_{-1}^2\Delta x_{-2}^3 \\
&+ 5\Delta x_{-1}^2\Delta x_{-2}^2\Delta x_{-3} + \Delta x_{-1}^2\Delta x_{-2}\Delta x_{-3}^2 - \Delta x_{-1}\Delta x_{-2}^4 - \Delta x_2\Delta x_{-2}^4 + 6\Delta x_{-1}^5)),
\end{aligned}
$$

$$
\begin{aligned}
d_a = &(2\Delta x_1 + \Delta x_2 + \Delta x_{-1})(\Delta x_1 + 2\Delta x_{-1} + \Delta x_{-2})(\Delta x_{-1} + 2\Delta x_{-2} + \Delta x_{-3}) \\
&\times (2\Delta x_1 + \Delta x_2 + 2\Delta x_{-1} + \Delta x_{-2})(\Delta x_1 + 2\Delta x_{-1} + 2\Delta x_{-2} + \Delta x_{-3}).
\end{aligned}
$$

Equation (2.19) indicates that $\mathrm{d}\bar{p}/\mathrm{d}x|_{x=x_i}$ is a first-order approximation of $\mathrm{d}\bar{u}/\mathrm{d}x|_{x=x_i}$ only if

$$
n_a/d_a = 1. \tag{2.20}
$$

□

The consistency condition, also known as geometric-conservativness [42] ($\frac{n_a}{d_a} = 1$), is satisfied only on some grid configurations like the arithmetic progression grid that we will study in this work. If we consider the grid as a geometric progression like $\Delta x_{-3} = a_0$, $\Delta x_{-2} = a_0 r$, ..., $\Delta x_2 = a_0 r^4$ (where r is the common ratio), we will get $\frac{n_a}{d_a} = \frac{4r}{(r+1)^2}$. The NCFDM scheme on the GP grid is at least first-order accurate when $r = 1$ or closer to one. Figure 2a shows the variation of $\frac{n_a}{d_a}$ for different values of r in GP grid. It is observed that the value of $\frac{n_a}{d_a}$ drops significantly when it deviates from $r = 1$.

The above condition ($n_a/d_a = 1$) may not be satisfied on a random grid. To test this, we have generated 1000 random grids of different mesh widths. The value of n_a/d_a for different samples are shown in Figure 2b. The mean of the distribution is 0.9237, and the standard deviation is 0.3375. From this, it is clear that the random grid cannot satisfy the condition. Only less than 0.1% of the grids satisfy $|(n_a/d_a) - 1| < 0.001$. We tested and showed this using a numerical test case in section 3.

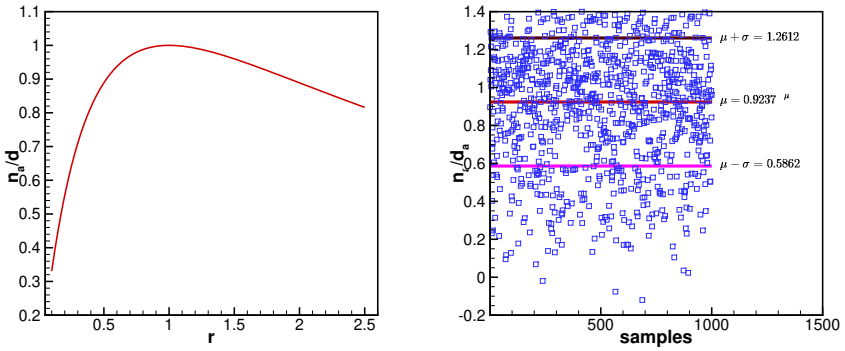

(a) (b)

Fig. 2: a) Variation of n_a/d_a for different r on GP grid. b) Variation of n_a/d_a on 1000 randomly generated grid

The NCFDM formulation in (2.16) can be simplified by choosing the grid configuration as AP. If we assume a linear progression of the mesh widths, namely $\Delta x_{-3} = a_0, \quad \Delta x_{-2} = a_0 + d, \quad \Delta x_{-1} = a_0 + 2d, \quad \Delta x_1 = a_0 + 3d \quad \text{and} \quad \Delta x_2 = a_0 + 4d$ in (2.16), we get

$$\left.\frac{\mathrm{d}\bar{p}}{\mathrm{d}x}\right|_{x=x_i} = \frac{M}{6\ (2a_0^4 + 17a_0^3 d + 52a_0^2 d^2 + 67a_0 d^3 + 30d^4)}, \tag{2.21}$$

where

$$\begin{aligned} M = {} & 6a_0^3\bar{u}_i + 4a_0^3\bar{u}_{i+1} - 12a_0^3\bar{u}_{i-1} + 2a_0^3\bar{u}_{i-2} + 65\bar{u}_i d^3 + 16\bar{u}_{i+1}d^3 - 111\bar{u}_{i-1}d^3 \\ & + 30\bar{u}_{i-2}d^3 + 106a_0\bar{u}_i d^2 + 47a_0^2\bar{u}_i d + 32a_0\bar{u}_{i+1}d^2 + 20a_0^2\bar{u}_{i+1}d \\ & - 175a_0\bar{u}_{i-1}d^2 - 82a_0^2\bar{u}_{i-1}d + 37a_0\bar{u}_{i-2}d^2 + 15a_0^2\bar{u}_{i-2}d, \end{aligned}$$

a_0 is the mesh width of the first cell, and d is the common increment in the AP series.

Theorem 3. *The accuracy of the scheme given in* (2.21) *at* $x = x_i$ *is first order.*

Proof. The Taylor series up to the second derivative term, is

$$\bar{u}(x_i + \tau) = \bar{u}(x_i) + \tau\frac{\mathrm{d}\bar{u}}{\mathrm{d}x}(x_i) + \frac{\tau^2}{2!}\frac{\mathrm{d}^2\bar{u}}{\mathrm{d}x^2}(x_i) + \mathcal{O}(\tau^3) \quad \text{as } \tau \to 0. \tag{2.22}$$

Expanding the computational molecules in terms of Taylor series gives

$$\begin{aligned}
\bar{u}_{i-2} &= \bar{u}(x_i) + (-2a_0 - 3d)\frac{\mathrm{d}\bar{u}}{\mathrm{d}x}(x_i) + \frac{(-2a_0-3d)^2}{2!}\frac{\mathrm{d}^2\bar{u}}{\mathrm{d}x^2}(x_i) \\
&\quad + \frac{(-2a_0-3d)^3}{3!}\frac{\mathrm{d}^3\bar{u}}{\mathrm{d}x^3}(x_i) + \frac{(-2a_0-3d)^4}{4!}\frac{\mathrm{d}^4\bar{u}}{\mathrm{d}x^4}(x_i) + \ldots, \\
\bar{u}_{i-1} &= \bar{u}(x_i) + (-a_0 - 2d)\frac{\mathrm{d}\bar{u}}{\mathrm{d}x}(x_i) + \frac{(-a_0-2d)^2}{2!}\frac{\mathrm{d}^2\bar{u}}{\mathrm{d}x^2}(x_i) \\
&\quad + \frac{(-a_0-2d)^3}{3!}\frac{\mathrm{d}^3\bar{u}}{\mathrm{d}x^3}(x_i) + \frac{(-a_0-2d)^4}{4!}\frac{\mathrm{d}^4\bar{u}}{\mathrm{d}x^4}(x_i) + \ldots, \\
\bar{u}_i &= \bar{u}(0), \\
\bar{u}_{i+1} &= \bar{u}(x_i) + (a_0 + 3d)\frac{\mathrm{d}\bar{u}}{\mathrm{d}x}(x_i) + \frac{(a_0+3d)^2}{2!}\frac{\mathrm{d}^2\bar{u}}{\mathrm{d}x^2}(x_i) \\
&\quad + \frac{(a_0+3d)^3}{3!}\frac{\mathrm{d}^3\bar{u}}{\mathrm{d}x^3}(x_i) + \frac{(a_0+3d)^4}{4!}\frac{\mathrm{d}^4\bar{u}}{\mathrm{d}x^4}(x_i) + \ldots.
\end{aligned} \tag{2.23}$$

When we substitute (2.23) in (2.16), we get

$$\begin{aligned}
\frac{\mathrm{d}\bar{p}}{\mathrm{d}x}(x_i) &= \frac{\mathrm{d}\bar{u}}{\mathrm{d}x}(x_i) - \frac{\mathrm{d}^2\bar{u}}{\mathrm{d}x^2}(x_i)\frac{d}{12} + \frac{\mathrm{d}^4\bar{u}}{\mathrm{d}x^4}(x_i)\frac{a_0^3}{12} + 59\frac{\mathrm{d}^4\bar{u}}{\mathrm{d}x^4}(x_i)\frac{a_0^2 d}{144} + 103\frac{\mathrm{d}^4\bar{u}}{\mathrm{d}x^4}(x_i)\frac{a_0 d^2}{144} \\
&\quad + \frac{\mathrm{d}^3\bar{u}}{\mathrm{d}x^3}(x_i)\frac{a_0 d}{4} + 65\frac{\mathrm{d}^4\bar{u}}{\mathrm{d}x^4}(x_i)\frac{d^3}{144} + 17\frac{\mathrm{d}^3\bar{u}}{\mathrm{d}x^3}(x_i)\frac{d^2}{36} + \text{h.o.t.}
\end{aligned} \tag{2.24}$$

The leading truncation error term is $-\frac{d}{12}\frac{\mathrm{d}^2\bar{u}}{\mathrm{d}x^2}(x_i)$, so the scheme is first-order accurate. □

When $d = 0$, the AP grid will be a uniform grid, so we will get a third-order accurate scheme. This can be proved by expanding each term using the Taylor series. Here, we shall derive it by evaluating the truncation term of the AP-formulation.

Theorem 4. *The accuracy of* (2.21) *is third order when* $d \to 0$.

Proof. The equation (2.21) is

$$\frac{\mathrm{d}\bar{u}}{\mathrm{d}x} = \frac{M}{6\,(2a_0^4 + 17a_0^3 d + 52a_0^2 d^2 + 67a_0 d^3 + 30d^4)},$$

Upon simplification using a Taylor expansion at $x = x_i$, we get

$$\begin{aligned}
\bar{u}_{i-2} &= \bar{u}(x_i) + (-2a_0 - 3d)\frac{\mathrm{d}\bar{u}}{\mathrm{d}x}(x_i) + \frac{(-2a_0-3d)^2}{2!}\frac{\mathrm{d}^2\bar{u}}{\mathrm{d}x^2}(x_i) \\
&\quad + \frac{(-2a_0-3d)^3}{3!}\frac{\mathrm{d}^3\bar{u}}{\mathrm{d}x^3}(x_i) + \frac{(-2a_0-3d)^4}{4!}\frac{\mathrm{d}^4\bar{u}}{\mathrm{d}x^4}(x_i) + \ldots, \\
\bar{u}_{i-1} &= \bar{u}(x_i) + (-a_0 - 2d)\frac{\mathrm{d}\bar{u}}{\mathrm{d}x}(x_i) + \frac{(-a_0-2d)^2}{2!}\frac{\mathrm{d}^2\bar{u}}{\mathrm{d}x^2}(x_i) \\
&\quad + \frac{(-a_0-2d)^3}{3!}\frac{\mathrm{d}^3\bar{u}}{\mathrm{d}x^3}(x_i) + \frac{(-a_0-2d)^4}{4!}\frac{\mathrm{d}^4\bar{u}}{\mathrm{d}x^4}(x_i) + \ldots, \\
\bar{u}_i &= \bar{u}(0), \\
\bar{u}_{i+1} &= \bar{u}(x_i) + (a_0 + 3d)\frac{\mathrm{d}\bar{u}}{\mathrm{d}x}(x_i) + \frac{(a_0+3d)^2}{2!}\frac{\mathrm{d}^2\bar{u}}{\mathrm{d}x^2}(x_i) \\
&\quad + \frac{(a_0+3d)^3}{3!}\frac{\mathrm{d}^3\bar{u}}{\mathrm{d}x^3}(x_i) + \frac{(a_0+3d)^4}{4!}\frac{\mathrm{d}^4\bar{u}}{\mathrm{d}x^4}(x_i) + \ldots.
\end{aligned} \tag{2.25}$$

When we substitute (2.25) in (2.16), we get

$$\begin{aligned}
\frac{\mathrm{d}\bar{u}}{\mathrm{d}x}(x = x_i) =& \frac{\mathrm{d}^4\bar{u}}{\mathrm{d}x^4}(x_i)\frac{a_0^3}{12} + 59\frac{\mathrm{d}^4\bar{u}}{\mathrm{d}x^4}(x_i)\frac{a_0^2 d}{144} + 103\frac{\mathrm{d}^4\bar{u}}{\mathrm{d}x^4}(x_i)\frac{a_0 d^2}{144} \\
&+ \frac{\mathrm{d}^3\bar{u}}{\mathrm{d}x^3}(x_i)\frac{a_0 d}{4} + 65\frac{\mathrm{d}^4\bar{u}}{\mathrm{d}x^4}(x_i)\frac{d^3}{144} + 17\frac{\mathrm{d}^3\bar{u}}{\mathrm{d}x^3}(x_i)\frac{d^2}{36} - \frac{\mathrm{d}^2\bar{u}}{\mathrm{d}x^2}(x_i)\frac{d}{12} + \text{h.o.t.}.
\end{aligned} \tag{2.26}$$

When we substitute $d = 0$ (or) very small value closer to zero, all the lower order terms in (2.26) vanishes and we get $\frac{\mathrm{d}^4\bar{u}}{\mathrm{d}x^4}(x_i)\frac{a_0^3}{12}$. The leading term in the truncation error equation is $\frac{a_0^3}{12}$, so the order of accuracy of the scheme is third-order, which is the maximum order of accuracy achieved for the first derivative formulation using $i-2$ to $i+1$ stencil. So, when we use an AP grid with a very small value of d, we may get the rate of convergence closer to the maximum theoretical order of accuracy on the uniform grid formulation. □

Theorem 4 is tested using several numerical test cases in section 3. We have seen by Theorem 2 that the NCFDM is not a first-order scheme. If we make the grid uniformly stretched, the order of accuracy can be improved. We can obtain an accuracy of the first order to the theoretical maximum order of the stencil based on the grid stretch ratio. This could be one of the reasons why we use uniform grids or gradually varying grids in computing tools. The order of accuracy issue only arises in the higher-order conservative discretization applied on a non-uniform grid. This may happen when we apply the methods developed for the uniform grid to a non-uniform grid. The finite difference method developed for non-uniform grid does not show any issue on any grid. The uniform grid is a sub-case of the non-uniform grid, so the non-uniform formulation should be reduced to the uniform grid formulation when we make the grid uniform. We shall test this by replacing the arbitrarily varying grid with a uniform grid in (2.16).

Table 1: Case 1 (computation of the derivative of $u(x) = \sin(x)$): L^2 error and rate of convergence of various schemes on non-uniform, AP, and uniform grids

	n	e_2 NFDM	R/c NFDM	Mean R/c NFDM	e_2 NCFDM	R/c NCFDM	Mean R/c NCFDM
NU-grid	101	1.2083E-4			1.0290E-1		
	201	1.4584E-5	3.0724		9.9700E-2	4.6000E-02	
	401	1.8307E-6	3.0047	3.0253	1.0560E-1	8.3400E-2	2.0366E-2
	801	2.2986E-7	2.9989		1.0070E-1	6.8300E-2	
AP-grid	101	1.2034E-4			4.3333E-4		
	201	1.4862E-5	3.0174		7.2333E-5	2.5827	
	401	1.8429E-6	3.0115	3.0117	1.2825E-5	2.0217	2.4739
	801	2.2938E-7	3.0061		2.5271E-6	2.3434	
U-grid	101	1.1468E-4			5.6950E-6		
	201	1.4497E-5	3.0053		3.6160E-7	3.0386	
	401	1.8204E-6	3.0210	3.0234	2.2780E-8	3.0210	3.0234
	801	2.2799E-7	3.0026		1.4300E-9	3.0107	

Theorem 5. *The discretization given in* (2.16) *equivalent to the finite difference scheme corresponds to the uniform grid when the uniform grid is applied.*

Proof. Substituting $\Delta x_{-2} = \Delta x_{-1} = \Delta x_1 = \Delta x_2 = \Delta x$ into (2.16) yields

$$\left.\frac{\mathrm{d}\bar{p}}{\mathrm{d}x}\right|_{x=x_i} = -\frac{1}{6\Delta x}\left(2\bar{u}_{i+1} + 3\bar{u}_i - 6\bar{u}_{i-1} + \bar{u}_{i-2}\right) + \mathcal{O}(\Delta x^3). \tag{2.27}$$

This is the third-order accurate finite difference method on a uniform grid. □

3 Numerical test cases

We now present the results of various discretizations on a uniform grid (the "U-grid"), a non-uniform grid ("NU-grid") and a grid with an arithmetic progression grid ("AP-grid") for the computation of derivatives, linear convection, linear convection-diffusion equation, the lid-driven cavity problem, and the Taylor-Green vortex problem. The uniform grid is generated by dividing the domain by 100, 200, 400, or 800 cells of equal size. The arbitrarily varying non-uniform grid is generated by randomly perturbing the uniform grid. The AP-grid is generated by making the grid size of AP series terms ($a_n = a_0 + nd$, where $a_0 = 1/150$).

3.1 Case 1: computation of the derivative of a given function

We evaluate the rate of convergence of the scheme constructed on a non-uniform grid by calculating the derivative of the smooth function $u(x) = \sin x$ with derivative $\mathrm{d}u/\mathrm{d}x = \cos x$. In various discretization approaches, the root mean square error (e_2) of the numerical solution is computed, and the rate of convergence is investigated. The solution of the derivative obtained using various techniques is shown in Figure 3 (a) and (c). Although the NFDM does not reveal any oscillations in the solution, the NCFDM does show oscillations. The reason for this is that when calculating

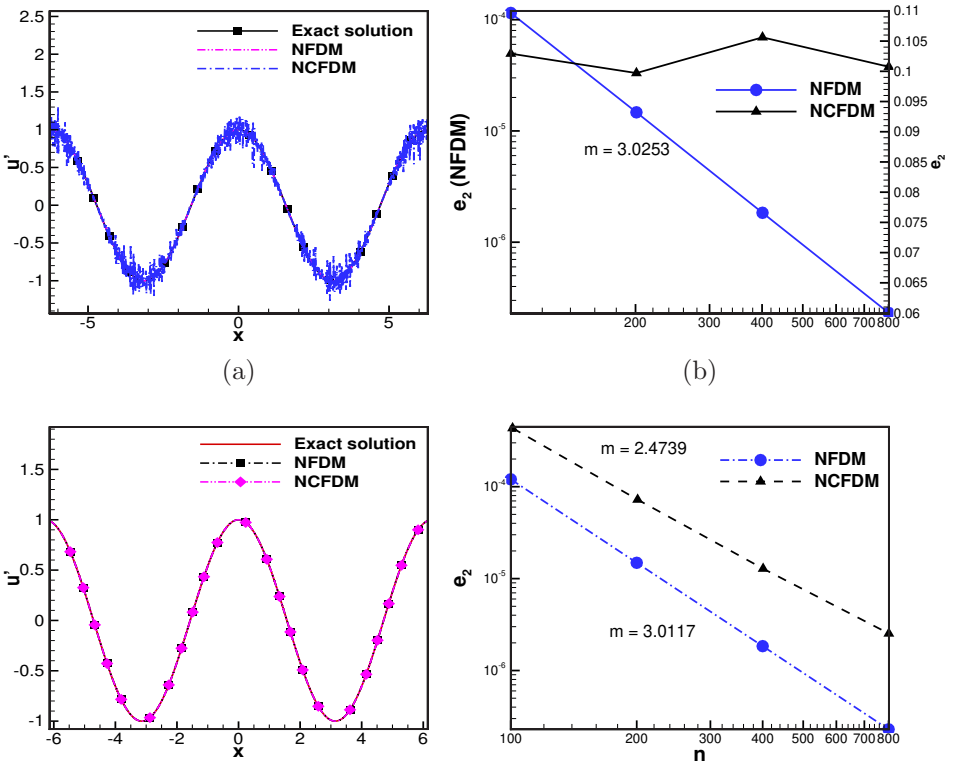

Fig. 3: Case 1: computation of the derivative of a given function using various schemes: (a) derivatives calculated on a non-uniform grid, (b) corresponding L^2 error versus number of grid points, (c) derivatives calculated on an AP grid, (d) corresponding L^2 error versus number of grid points.

cell-centered values, we employ cell-average interpolation, but when calculating cell-interface values, we use standard interpolation. On the uniform grid, this will result in higher-order accurate formulation, while on randomly stretched grids, it will result in lower-order convergence. The rate of convergence of various discretization is depicted in Figures 3 (b) and (d). The NFDM can achieve the desired rate of convergence, whereas others do not with grid refinement.

The derivative calculation on AP-grid is shown in Figure 3 (c). Although there are no oscillations in the AP-grid, the conservative discretization shows a slower rate of convergence than the NFDM. It is noteworthy that conservative discretizations on a non-uniform grid are not even first-order accurate, but all the schemes presented in this work exhibit uniform convergence (see Figure 3 (d)). The rate of convergence obtained on the AP-grid is higher than the order of accuracy calculated in Theorem 3 (which

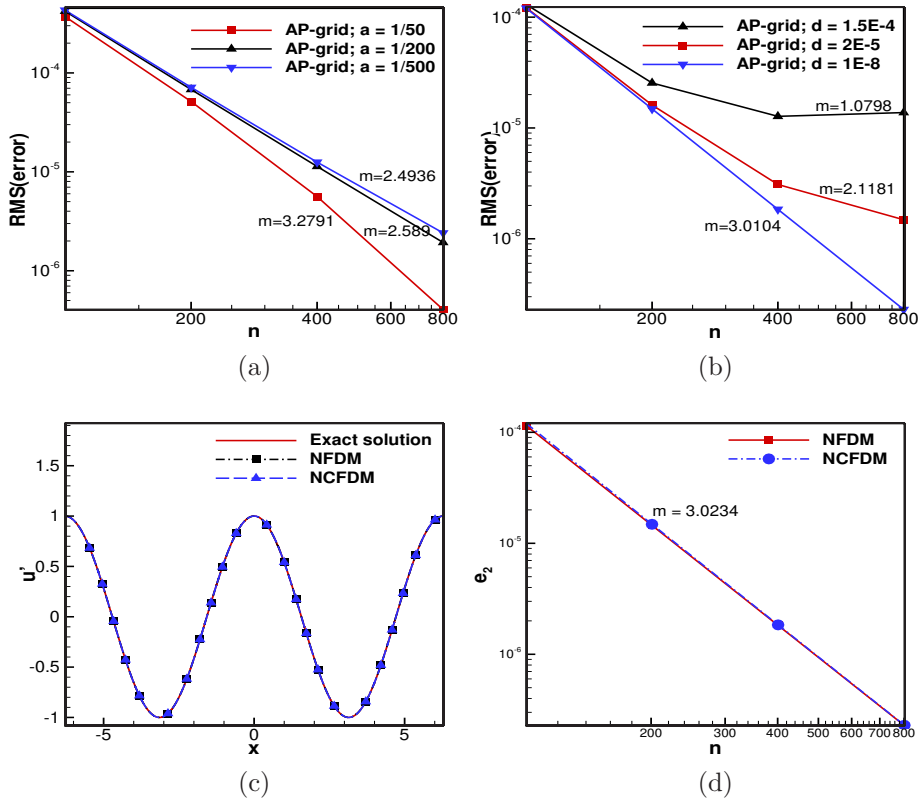

Fig. 4: Case 1: computation of the derivative of a given function using various schemes: (a) the effect of the value of a on an AP-grid, (b) the effect of the value of d on an AP grid, (c) derivatives calculated on a uniform grid, (d) L^2 error versus number of grid points.

is one). We already studied in Theorem 4 that when we decrease d, we may get convergence up to the order of accuracy corresponding to the uniform grid. Figures 4 (c) and (d) show the variation of rate of convergence for different values of a and d. When we reduce a, the rate of convergence reduces and becomes a saturated value of about 2.5. A small value of a means that the points of the AP-grid approach a uniform grid on which we got the rate of convergence about 3. Likewise, when we increase the value of d (that means the grid stretching is high), the rate of convergence shows a non-linear behavior. For this case, the rate of convergence is reduced to 1.0798 when $d = 1.5 \times 10^{-4}$, which is closer to the theoretical estimate.

Figure 4 (c) illustrates the solution on a uniform grid, and the corresponding rate of convergence is presented in Figure 4 (d). When we make the grid uniform, all of the schemes can deliver a rate of convergence equal to the stencil's highest order of

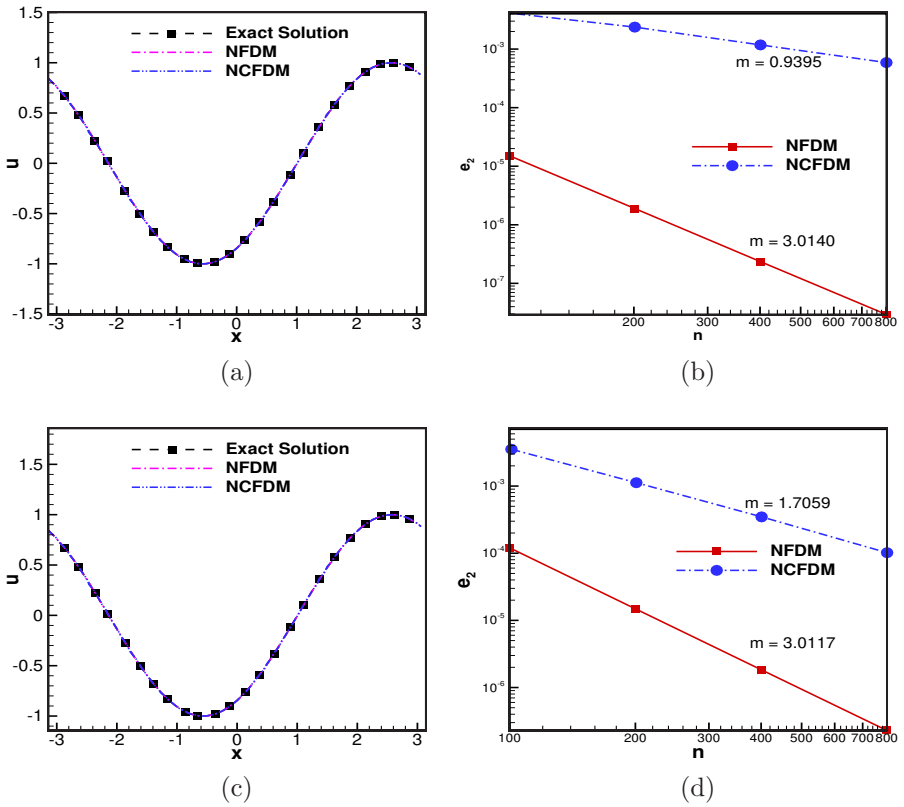

Fig. 5: Case 2 (linear advection equation): (a) numerical solutions on a non-uniform grid at simulated time $T = 1$, (b) corresponding L^2 errors versus number of grid points, (c) numerical solutions on an AP grid at simulated time $T = 1$, (d) corresponding L^2 errors versus number of grid points.

accuracy, which is three. Table 1 shows the L^2 error, rate of convergence, and the average rate of convergence on the three grids.

3.2 Case 2: the linear advection equation

The linear convection equation is:

$$\frac{\partial u}{\partial t} + c\frac{\partial u}{\partial x} = 0. \tag{3.1}$$

We study the linear convection equation (3.1) along with the initial condition $u(x, 0) = \sin x$. The problem is solved over the domain $[-\pi, \pi]$ with periodic boundary conditions and the density is convected with velocity $c = 1$. To calculate the rate of convergence, the domain is subdivided into 101, 201, 401, and 801 grid points, and CFL number

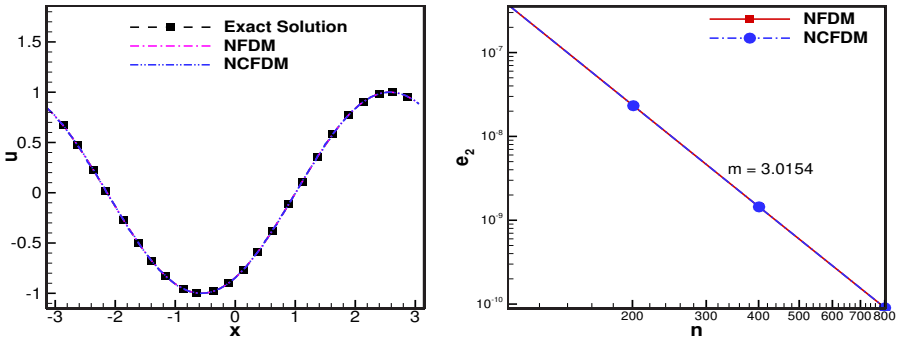

(a) (b)

Fig. 6: Case 2 (linear advection equation): (a) numerical solutions on a uniform grid at simulated time $T = 1$, (b) corresponding L^2 error versus number of grid points.

Table 2: Case 2 (linear advection equation): L^2 error and rate of convergence of various schemes on non-uniform, AP, and uniform grids

	n	e_2 NFDM	R/c NFDM	Mean R/c NFDM	e_2 NCFDM	R/c NCFDM	Mean R/c NCFDM
NU-grid	101	1.5087E-5			4.1184E-3		
	201	1.8940E-6	3.0153		2.3715E-3	0.8020	
	401	2.3486E-7	3.0224	3.0140	1.1776E-3	1.0135	0.9395
	801	2.9380E-8	3.0043		5.8832E-4	1.0030	
AP-grid	101	1.2034E-4			3.5353E-3		
	201	1.4862E-5	3.0174		1.1229E-3	1.6545	
	401	1.8429E-6	3.0115	3.0117	3.4773E-4	1.6912	1.7059
	801	2.2938E-7	3.0061		1.0181E-4	1.7720	
U-grid	101	1.4689E-5			1.4689E-05		
	201	1.8366E-6	3.0212		1.8366E-06	3.0212	
	401	2.2815E-7	3.0198	3.0154	2.2815E-07	3.0198	3.0154
	801	2.8519E-8	3.0053		2.8519E-08	3.0053	

0.4 is used. The L^2 error is calculated at simulated time $T = 1$. For the time integration, we utilized HRK41 method [21], and for the spatial discretization, we employed various non-uniform discretization methods described in this work. Figure 5 (a) shows the solution of the linear convection equation using the non-uniform grid. Unlike spatial derivative calculations, oscillations are not severe for conservative discretization. Interestingly, the conservative schemes, which are not even theoretically first-order accurate, have a rate of convergence that is slightly less than one. Figure 5 (c) shows the solution on the AP-grid. On this grid, the conservative discretization also exhibits a consistent convergence rate of greater than 1.6 (see Figure 5 (d)). Figure 6 (a) shows the solution on a uniform grid. As expected, all schemes exhibit a rate of convergence

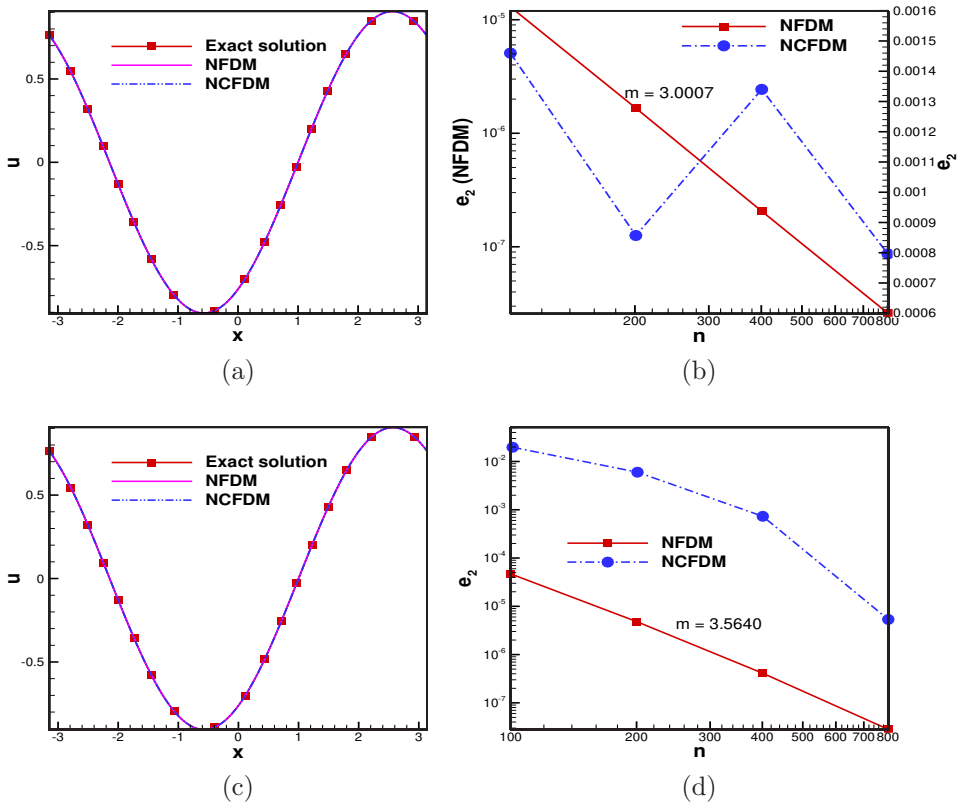

Fig. 7: Case 3 (linear convection-diffusion equation): numerical solutions using NFDM and NCFDM at simulated time $T = 1$ with CFL $= 0.3$ and Pe $= 0.3$: (a) numerical solutions on a non-uniform grid, (b) corresponding approximate L^2 errors versus the number of grid points, (c) numerical solutions on an AP grid, (d) corresponding approximate L^2 errors versus number of grid points.

that is nearly identical to the stencil's maximum order of accuracy on this grid. The L^2 errors on the different grids are tabulated in Table 2.

The CFDM and FDM are reduced to the same formulation on a uniform grid, and the results of those inferences are the same on a uniform grid.

3.3 Case 3: linear convection-diffusion equation

The convection-diffusion equation is

$$\frac{\partial u}{\partial t} + c\frac{\partial u}{\partial x} = \varepsilon \frac{\partial^2 u}{\partial x^2}. \tag{3.2}$$

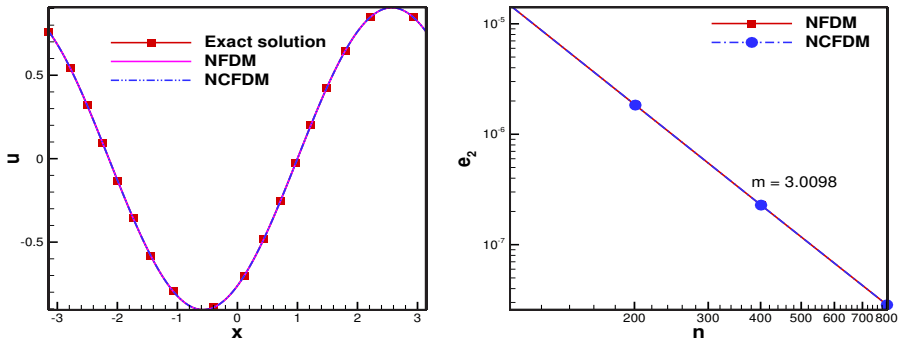

(a) (b)

Fig. 8: Case 3 (linear convection-diffusion equation): numerical solutions using NFDM and NCFDM at simulated time $T = 1$ with CFL $= 0.3$ and Pe $= 0.3$: (a) numerical solutions on a uniform grid, (b) corresponding approximate L^2 errors versus number of grid points.

Table 3: Case 3 (linear convection-diffusion equation): L^2 error and rate of convergence of various schemes on non-uniform, AP, and uniform grids

	n	e_2 NFDM	R/c NFDM	Mean R/c NFDM	e_2 NCFDM	R/c NCFDM	Mean R/c NCFDM
NU-grid	101	1.29E-5			1.46E-3		
	201	1.66E-6	2.9832		8.57E-4	0.7769	
	401	2.05E-7	3.0279	3.0007	1.34E-3	0.6431	0.2941
	801	2.59E-8	2.9909		7.96E-4	0.7488	
AP-grid	101	4.68E-5			1.97E-2		
	201	4.82E-6	3.2786		6.00E-3	1.7138	
	401	4.14E-7	3.5434	3.5640	7.32E-4	3.0345	3.9491
	801	2.83E-8	3.8699		5.34E-2	-7.099	
U-grid	101	1.31E-5			1.31E-5		
	201	1.65E-6	3.0128		1.65E-6	3.0129	
	401	2.06E-7	3.0113	3.0098	2.06E-7	3.0114	3.0098
	801	2.58E-8	3.0052		2.58E-8	3.0052	

On various grids, we evaluated the performance of different methods developed in this work on the linear convection-diffusion equation (3.2) with $c = 1$ and $\varepsilon = 0.1$. The initial condition used is $u(x, 0) = \sin(x)$ with periodic boundary conditions. The exact solution for this test case is $u(x, t) = \sin(x - ct) \exp^{-\epsilon t}$. To investigate the rate of convergence, the domain is divided into 100, 200, 400, and 800 cells. The fourth-order NFDM is used to discretize the diffusion term. Though there are no significant oscillations are present in the solution (see Figure 7 (a)), the conservative discretization unable to give a uniform rate of convergence (see Figure 7 (b)). They are not only

Table 4: Cases 1 to 3: summary of the performance of different schemes on uniform (U), non-uniform (NU), and arithmetic progression (AP) grid

Method	Grid	R/c on du/dx	Oscill.	R/c on LC	Oscill.	R/c on LCD	Oscill.
NFDM	NU-grid	3.0253 (3)	No	3.0140 (3)	No	3.0007 (3)	No
NFDM	AP-grid	3.0117 (3)	No	3.0117 (3)	No	3.5640 (3)	No
NFDM	U-grid	3.0234 (3)	No	3.0154 (3)	No	3.0098 (3)	No
NCFDM	NU-grid	0.0103 (3)	Yes	0.9395 (3)	No	0.2941 (3)	No
NCFDM	AP-gid	2.4739 (3)	No	1.7059 (3)	No	3.9491 (3)	No
NCFDM	U-grid	3.0234 (3)	No	3.0154 (3)	No	3.0098 (3)	No

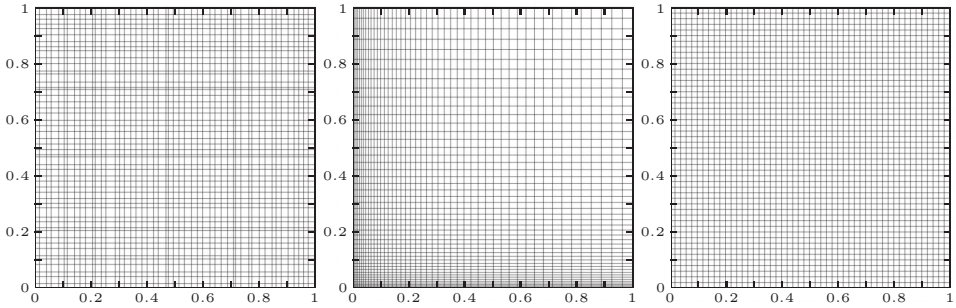

(a) NU-grid (b) AP-grid (c) U-grid

Fig. 9: Case 4 (lid-driven cavity problem): sample 51× 51 grid configurations

unable to produce a uniform rate of convergence on the NU-grid but also on the AP-grid (see Figure 7 (d)). Similar to other test cases, they produce the expected rate of convergence on the uniform grid (see Figure 8 (b)). Table 3 shows the L^2 error on the various grids, and Table 4 summarizes the performance of schemes for Cases 1 to 3 on different grids. In that table, the last column, the "oscill." column, indicates whether there are oscillations in the solution or not. Here LC refers to the linear convection equation, and LCD refers to the linear convection-diffusion equation. On the AP-grid, NFDM exhibits super-convergence.

3.4 Case 4: lid-driven cavity problem

The lid-driven cavity is a standard test case to validate the numerical scheme. Here, we have used stream function-vorticity formulation to solve this test case.

$$\nabla^2\vec{\psi} = -\vec{\omega},$$
$$\frac{\partial\vec{\omega}}{\partial t} + (\vec{V}\cdot\nabla)\vec{\omega} = \frac{1}{\mathrm{Re}}\nabla^2\vec{\omega}.$$

The stream function $\vec{\psi}$ and the velocity $\vec{V}$ are related by $\vec{V} = \nabla\times\vec{\psi}$. In two space dimensions, $\vec{\psi} = (0, 0, \psi)^{\mathrm{T}}$. Velocity and vorticity are connected by the relation $\vec{\omega} =$

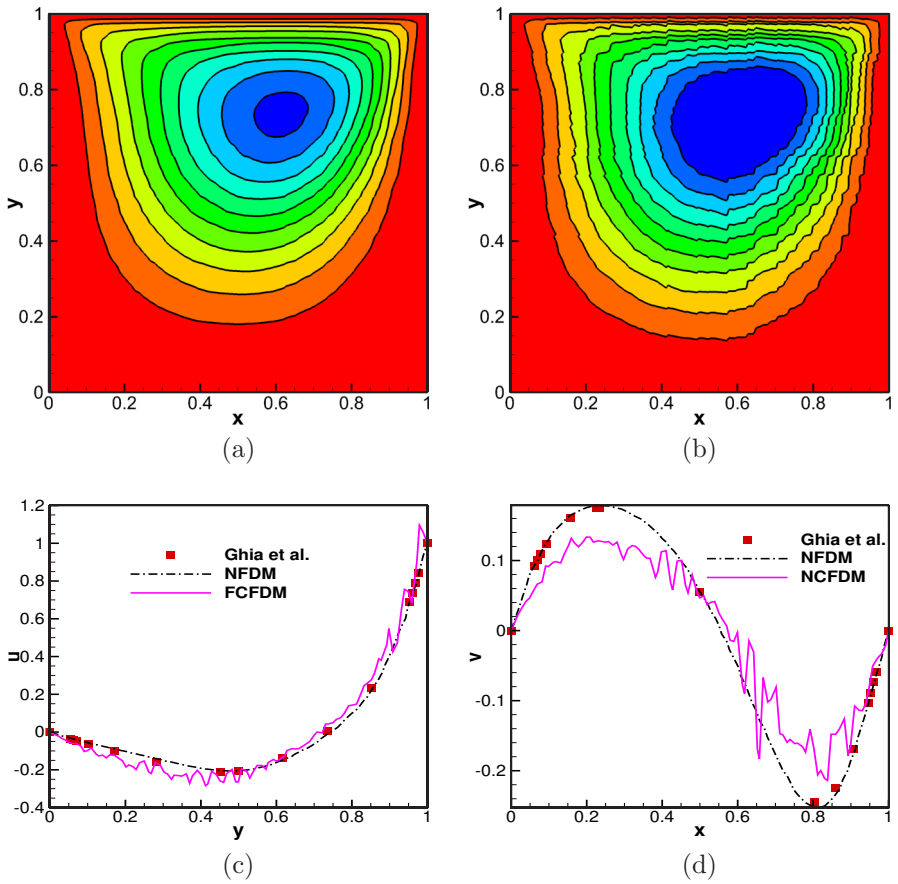

Fig. 10: Case 4 (lid-driven cavity problem): numerical solution at simulated time $T = 50$ on an arbitrarily perturbed non-uniform grid by (a) NFDM and (b) NCDFM schemes and (c), (d) comparison with the results by Ghia et al. [43].

$\nabla \times \vec{V}$. The test case is solved at a Reynolds number 100 on 101×101 grid configuration over the domain $[0, 1] \times [0, 1]$. The convection terms are discretized using NCFDM and NFDM. The diffusion terms are discretized using a fourth-order finite difference central scheme. The time advancement is carried out using the explicit Euler method. The top surface of the lid is moved with a unit velocity. On the other surfaces, a no-slip boundary condition is imposed. More details of the problem and the grid sensitivity and error dynamics over time are found in [44].

The problem is solved up to simulated time 50 s and the performance of the different schemes is compared with the experimental results by Ghia et al. [43]. Figures 10 (a) and (b) show the stream function contour of NFDM and NCFDM, respectively, on an arbitrarily perturbed non-uniform grid. From Figure 10, it is clear that NCFDM shows oscillations in the solution (see Figure 10 (a)) but NFDM does not show any oscillations (see Figure 10 (b)). Figure 10 (c) shows the x-velocity at location $y = 0.5$

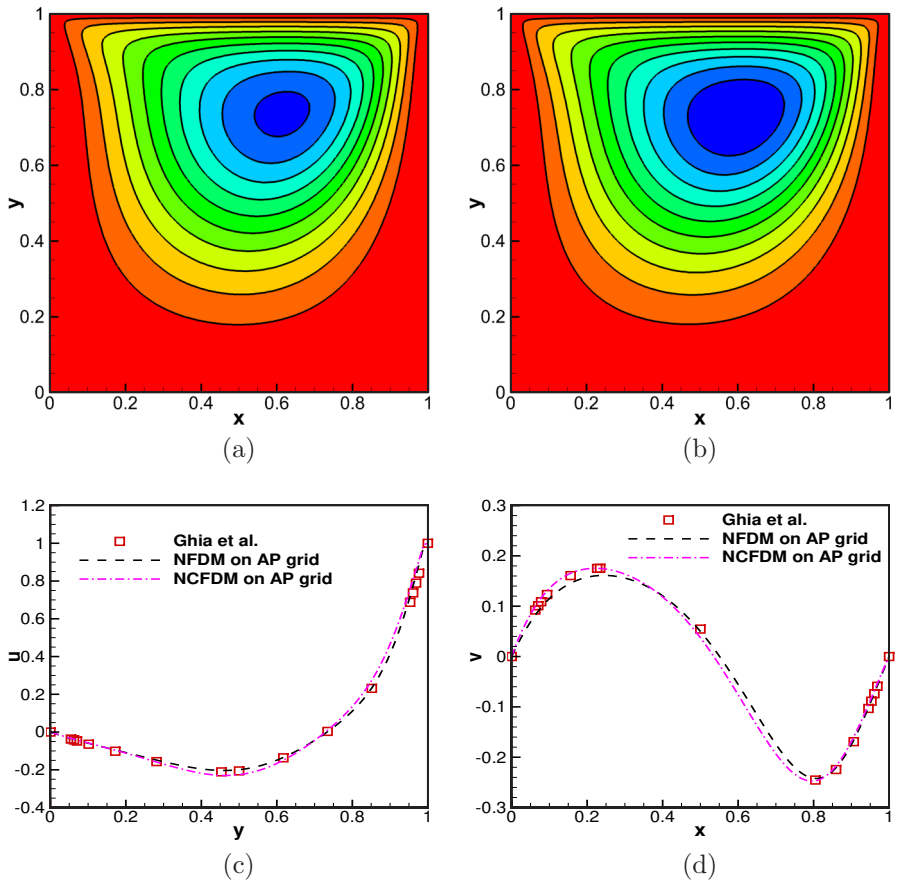

Fig. 11: Case 4 (lid-driven cavity problem): numerical solution at simulated time $T = 50$ on an AP-grid by (a) NFDM and (b) NCDFM schemes and (c), (d) comparison with the results by Ghia et al. [43].

of NFDM, CFDM and Ghia et al. Similarly, the y-velocity at $x = 0.5$ is presented in Figure 10 (d). In both the velocity profiles, NCFDM shows oscillation but NFDM is not showing oscillations. When we replace the non-uniform grid by a gradually varying grid like the AP grid, oscillations disappear. Figures 11 (a) and (b) show the stream function contour on an AP-grid where no oscillations are observed in the solution. That is verified by cutting a plane at $x = 0.5$ and $y = 0.5$ in u- and v-velocity contours. As expected, no oscillations are observed in Figure 11 which supports our conjecture that NCFDM demands a smoothly varying grid but NFDM does not demand a smoothly varying grid. Because both the schemes are reduced to the same formulation, there is no difference in the results of the NCFDM and NFDM on a uniform grid (see Figure 12).

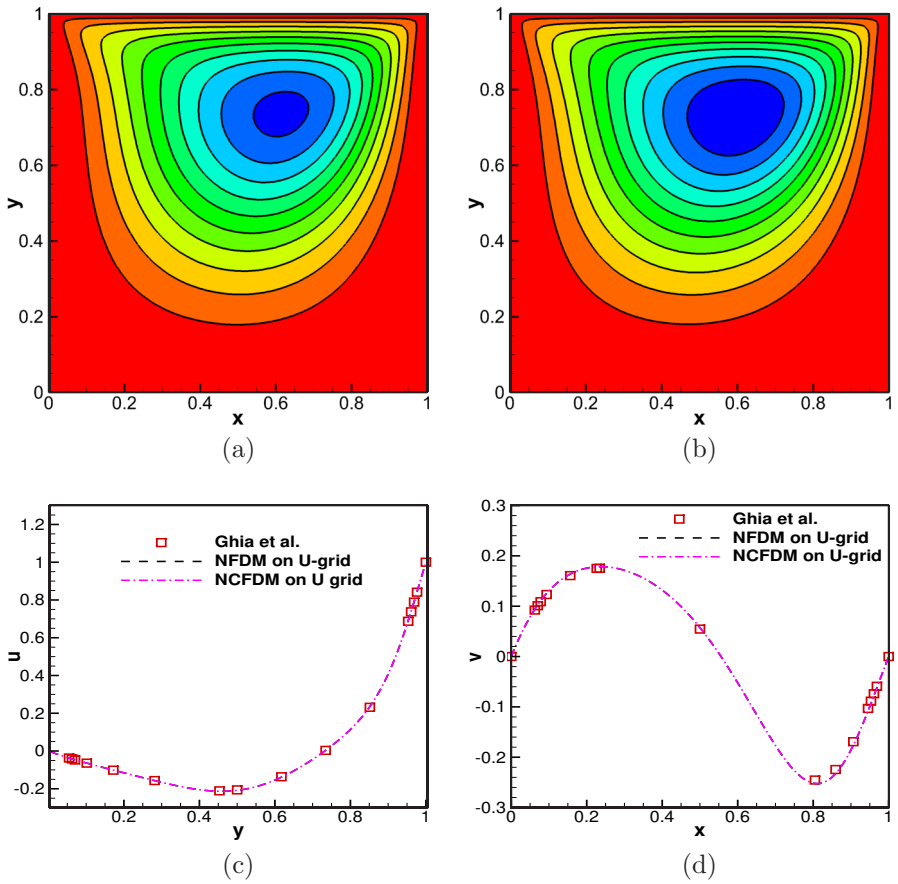

Fig. 12: Case 4 (lid-driven cavity problem): numerical solution at simulated time $T = 50$ on a uniform grid by (a) NFDM and (b) NCDFM schemes and (c), (d) comparison with the results by Ghia et al. [43].

3.5 Case 5: Taylor-Green vortex problem

The Taylor-Green vortex problem is another benchmark problem for the Navier-Stokes equation proposed by Taylor and Green [45]. The same discretization procedure used in the lid-driven cavity is used here but the domain size is changed to $[0, 2\pi] \times [0, 2\pi]$ to allow for an easy application of periodic boundary conditions. The domain is divided into 101×101 grid points with the initial condition

$$\psi(x, y, 0) = \sin x \sin y, \qquad \omega(x, y, 0) = 2 \sin x \sin y.$$

The exact solution for this problem is [34]

$$\psi(x, y, t) = \sin x \sin y \; F(t), \qquad \omega = 2 \sin x \sin y F(t),$$

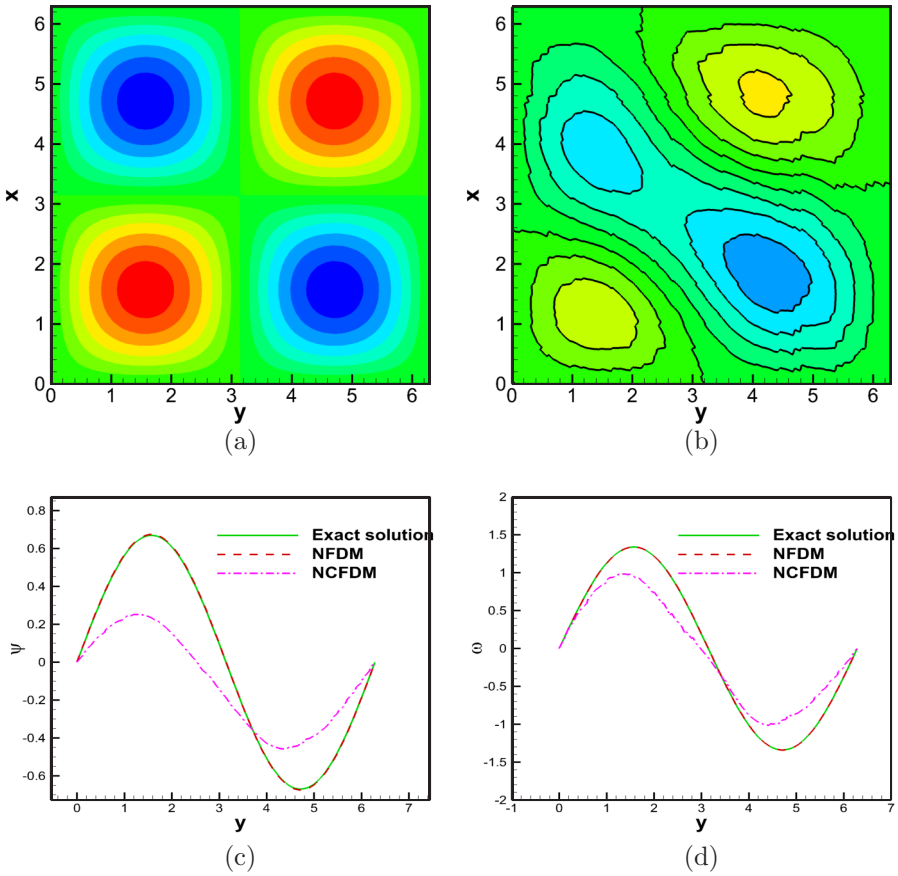

Fig. 13: Case 5 (Taylor-Green vortex problem): numerical solution by NFDM and NCDFM schemes at simulated time $T = 50$ on a non-uniform grid: (top) contours of the stream function produced by (a) the NFDM scheme, (b) the NCDFM scheme, (c) comparison of the stream function at $x = 0.25$ with the exact solution, (d) comparison of the vorticity at $x = 0.25$ with the exact solution.

$$\text{where} \quad F(t) = \exp(2\nu t), \quad \nu = 2\pi/\text{Re}.$$

We here use the Reynolds number $\text{Re} = 1000$. More details about the instability analysis of this problem and the mechanism which trigger the non-linear instability by the evolution of disturbance mechanical energy and enstrophy are presented in [46]. Here also the performance of the NCFDM and NFDM is tested on the non-uniform grid, AP-grid and uniform grid. Figures 13 (a) and (b) show the stream-function contour of NFDM and NCFDM, respectively. From Figure 13 (b) it is clear that NCFDM is unable to resolve the vortices present in the solution on a non-uniform grid which is also reflected on the line plots of steam function and vorticity (see Figure 13).

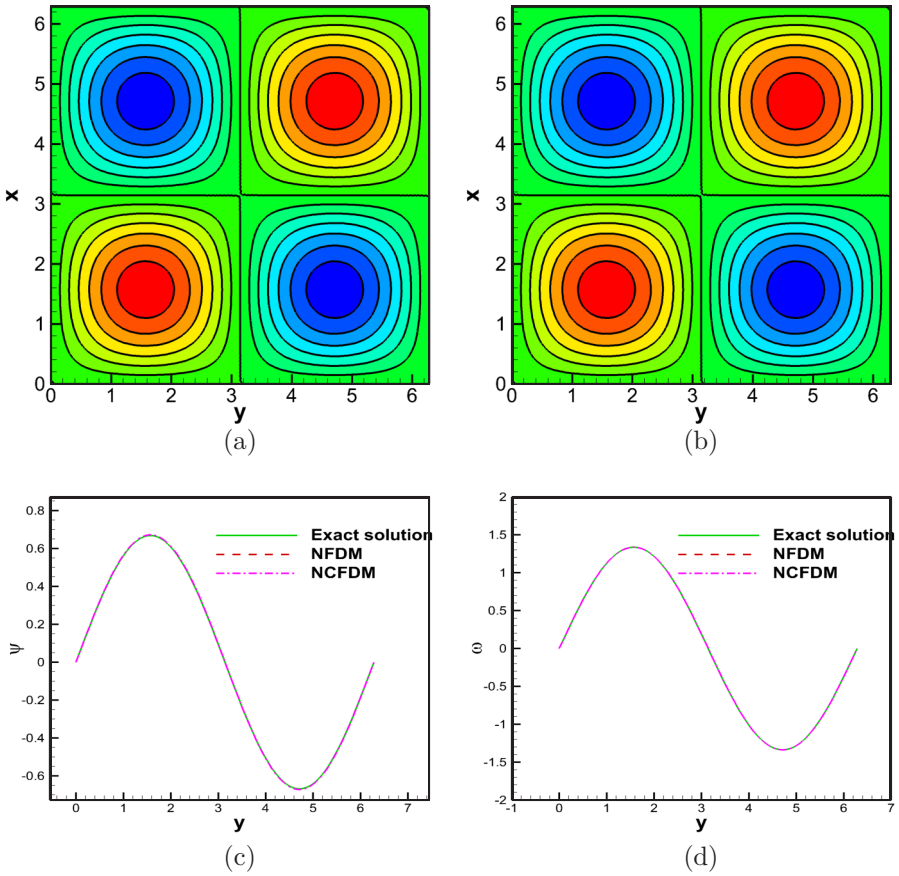

Fig. 14: Case 5 (Taylor-Green vortex problem): numerical solution by NFDM and NCDFM schemes at simulated time $T = 50$ on an AP-grid: (top) contours of the stream function produced by (a) the NFDM scheme, (b) the NCDFM scheme, (c) comparison of the stream function at $x = 0.25$ with the exact solution, (d) comparison of the vorticity at $x = 0.25$ with the exact solution.

The stream function and vorticity at location $x = 0.25$ are shown in Figures 13 (c) and (d), respectively, on a non-uniform grid. From Figure 13, it is clear that the oscillations are observed in NCFDM but NFDM is not showing any oscillations. In addition, the amplitude of the solution also diffused and deviated away from the exact solution in the case of NCFDM. Similarly to previous observations, these oscillations disappear when we use an AP-grid or a uniform grid. Figures 14 (b) and 15 (b) show the stream function contour of the present test case on an AP-grid and a uniform grid, respectively. Similarly, the stream function and vorticity plot of an AP-grid at location $x = 0.25$ are shown in Figure 14; for a uniform grid, results are shown in Figure 15.

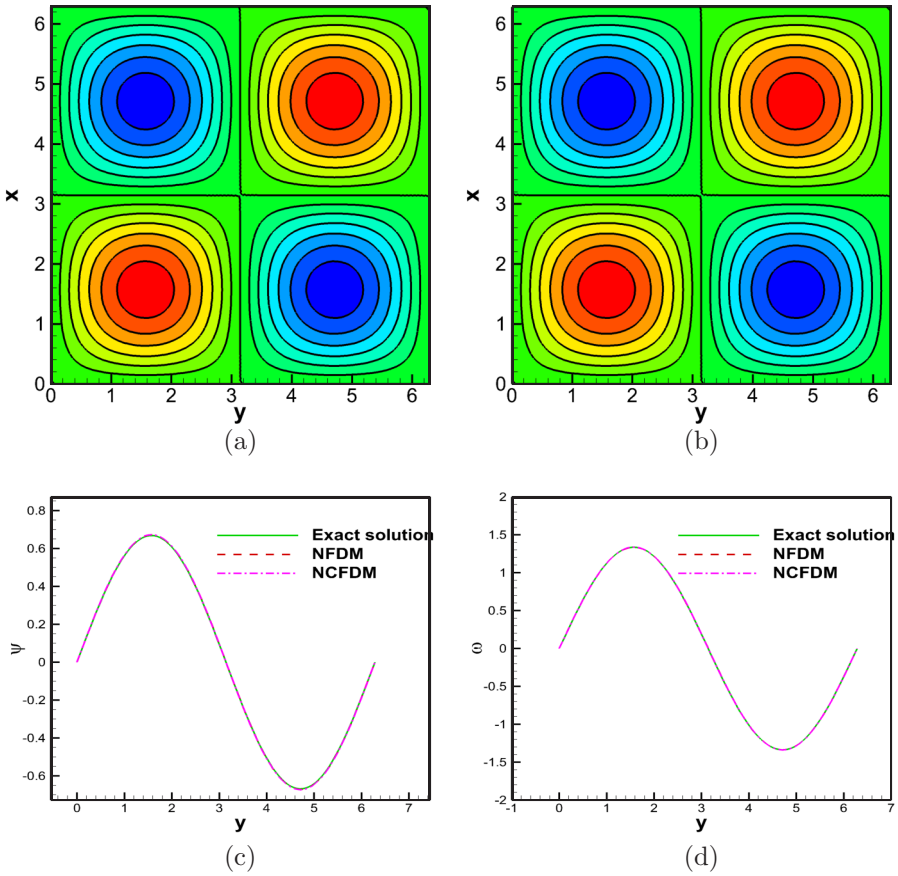

Fig. 15: Case 5 (Taylor-Green vortex problem): numerical solution by NFDM and NCDFM schemes at simulated time $T = 50$ on a uniform grid: (top) contours of the stream function produced by (a) the NFDM scheme, (b) the NCDFM scheme, (c) comparison of the stream function at $x = 0.25$ with the exact solution, (d) comparison of the vorticity at $x = 0.25$ with the exact solution.

As expected, there are no oscillations in the solution using NCFDM, when we apply this discretization on a gradually varying grid or uniform grid. These oscillations arise in NCFDM for two potential reasons, One is the multi-cell averaging associated with the higher-order conservative discretization, and the other is usage of cell-average interpolation to calculate cell-centre values and standard point-based interpolation to calculate the cell-interface value in the conservative discretization.

4 Conclusions

When we numerically solve the transport equation over complex geometry, the unstructured mesh is preferred over the uniform mesh. On an unstructured grid, the grid stretch/contraction ratio plays an important role in the accuracy of the solution. We should use a gradually shifting grid for better convergence and more accurate results. In the present study, we investigated the effect of the rate of convergence and order of accuracy on an arbitrary shifting non-uniform grid in the Cartesian grid when we use conservative framework. Determining the theoretical order of accuracy of FVM on an unstructured grid is challenging, but it is relatively simple on a Cartesian grid. In this work, we focused on CFDM because FVM and CFDM are reduced to the same formulation on a Cartesian grid. We have theoretically shown that the order of accuracy of CFDM on any arbitrarily varying non-uniform grid solely depends on the grid used. For an arbitrary non-uniform grid, the scheme may not always a first-order accurate. The condition required to achieve minimum first-order accuracy on an arbitrary non-uniform grid is also present. Because the derivation procedure is lengthy and complex, symbolic computational tools were utilised. Due to skewness, non-orthogonality, and significant inaccuracy in gradient calculations and interpolations, the unstructured mesh has higher errors than the Cartesian grid. So FVM on the non-Cartesian mesh is likely to have more errors on an unstructured grid than on the Cartesian grid.

The rate of convergence and order of accuracy of NFDM and NCFDM are studied on a uniform grid, non-uniform grid, and arithmetic progression grid on simple derivative calculation, linear advection equation, and linear advection-diffusion equation. As expected, NCFDM shows poor convergence or results on the non-uniform grid. Surprisingly, this higher-order NCFDM has shown a uniform convergence rate of slightly lower than one for the linear advection equation. They produced a higher rate of convergence on the AP grid than on an arbitrarily shifting grid. We have theoretically and numerically shown that the rate of convergence on the AP-grid can be improved by adjusting the value of d. On the uniform grid, they produced the expected rate of convergence for all the test cases equivalent to NFDM schemes.

Apart from linear equations, we have also tested the performance of NCFDM and NFDM on non-linear problems with various grid configurations like the random non-uniform grid, AP-grid, and uniform grid. The test cases we considered are the lid-driven cavity and the Taylor-Green vortex problem. Similar to linear test cases, NCFDM produced oscillations in the solution, but NFDM did not produce any oscillations. As expected, no oscillations are observed on the uniform grid and AP grid. The oscillations that arise in the higher-order NCFDM may be because we use two different interpolation polynomials: cell-averaged stencil to calculate the cell-center value and point-wise interpolation for cell-interface calculation. This procedure helps achieve higher-order accuracy on uniform mesh because of the index-shifting property. This high order cannot be attained on random non-uniform grids. The cell-averaged polynomial is widely used in deriving weighted essentially non-oscillatory schemes to get higher-order convergence on a uniform grid. The proposed limitation is also valid for the sub-stencil derivation of the WENO formulation. This may limit the extension of explicit formulation of the conservative WENO scheme on the non-uniform grid based on multi-cell averaging. The scope of the present work is restricted to Cartesian

mesh with orthogonal faces. In the future, the proof will be extended to faces that have non-orthogonal edges so that errors due to orthogonality and skewness can be quantified.

Availability of data and materials. The codes for conservative FDM and FDM for the non-uniform grid are available in the https://github.com/AGN000/Conservative-NFDM/tree/main. Other codes can be obtained from the authors based on reasonable request.

Acknowledgments. The author Raimund Bürger acknowledges support by project MATH-Amsud 22-MATH-05 "NOTION: NOn-local conservaTION laws for engineering, biological and epidemiological applications: theoretical and numerical" and from ANID (Chile) through Fondecyt project 1210610; Anillo project ANID/ACT210030; Centro de Modelamiento Matemático (CMM), project FB210005 of BASAL funds for Centers of Excellence; and CRHIAM, project ANID/FONDAP/15130015.

The author Samala Rathan is supported by NBHM, DAE, India (Ref. No. 02011/46/2021 NBHM(R.P.)/R & D II/14874).

Conflict of interest. The authors declare that there is no conflict of interest in the manuscript.

References

[1] Anderson, J.D., Degrez, G., Dick, E., Grundmann, R.: Computational Fluid Dynamics: an Introduction. Springer, Heidelberg (2013)

[2] LeVeque, R.J.: Finite Volume Methods for Hyperbolic Problems. Cambridge Texts in Applied Mathematics, p. 558. Cambridge University Press, Cambridge, UK (2002). https://doi.org/10.1017/CBO9780511791253

[3] Neelan, A.A.G., Nair, M.T., Bürger, R.: Three-level order-adaptive weighted essentially non-oscillatory schemes. Results Appl. Math. **12**, 100217 (2021) https://doi.org/10.1016/j.rinam.2021.100217

[4] Baeza, A., Bürger, R., Mulet, P., Zorío, D.: Central WENO schemes through a global average weight. J. Sci. Comput. **78**(1), 499–530 (2019)

[5] Shu, C.-W., Osher, S.: Efficient implementation of essentially non-oscillatory shock-capturing schemes. J. Comput. Phys. **77**(2), 439–471 (1988) https://doi.org/10.1016/0021-9991(88)90177-5

[6] Roe, P.L.: Error estimates for cell-vertex solutions of the compressible Euler equations. NASA contractor report ; 178235 (1987)

[7] Barbeiro, S.: Supraconvergent cell-centered scheme for two dimensional elliptic problems. Appl. Numer. Math. **59**(1), 56–72 (2009) https://doi.org/10.1016/j.apnum.2007.11.021

[8] Barbeiro, S., Ferreira, J.A., Grigorieff, R.D.: Supraconvergence of a finite difference scheme for solutions in $h^s(0,l)$. IMA J. Numer. Anal. **25**(4), 797–811 (2005) https://doi.org/journal="JournalofComputationalPhysics",

[9] Bouche, D., Ghidaglia, J.-M., Pascal, F.: Error estimate and the geometric corrector for the upwind finite volume method applied to the linear advection equation. SIAM J. Numer. Anal. **43**(2), 578–603 (2005) https://doi.org/10.1137/040605941 https://doi.org/10.1137/040605941

[10] De Hoog, F., Jackett, D.: On the rate of convergence of finite difference schemes on nonuniform grids. J. Austral. Math. Soc. Ser. B Appl. Math. **26**(3), 247–256 (1985) https://doi.org/10.1017/S0334270000004495

[11] Despres, B.: Lax theorem and finite volume schemes. Math. Comp. **73**(247), 1203–1234 (2004)

[12] Eriksson, S., Nordström, J.: Analysis of the order of accuracy for node-centered finite volume schemes. Appl. Numer. Math. **59**(10), 2659–2676 (2009) https://doi.org/10.1016/j.apnum.2009.06.001

[13] Ferreira, J.A., Grigorieff, R.D.: On the supraconvergence of elliptic finite difference schemes. Appl. Numer. Math. **28**(2), 275–292 (1998) https://doi.org/10.1016/S0168-9274(98)00048-8

[14] Forsyth, P.A., Sammon, P.H.: Quadratic convergence for cell-centered grids. Appl. Numer. Math. **4**(5), 377–394 (1988) https://doi.org/10.1016/0168-9274(88)90016-5

[15] Kreiss, H.-O., Manteuffel, T.A., Swartz, B., Wendroff, B., White, A.B.: Supra-convergent schemes on irregular grids. Math. Comp. **47**(176), 537–554 (1986)

[16] Pascal, F.: On supra-convergence of the finite volume method for the linear advection problem. In: ESAIM: Proceedings, vol. 18, pp. 38–47 (2007). EDP Sciences

[17] Thomas, J.L., Diskin, B., Rumsey, C.L.: Towards verification of unstructured-grid solvers. AIAA J. **46**(12), 3070–3079 (2008)

[18] Neelan, A.A.G., Nair, M.T.: Hybrid finite difference-finite volume schemes on non-uniform grid. In: Singh, M.K., Kushvah, B.S., Seth, G.S., Prakash, J. (eds.) Applications of Fluid Dynamics, pp. 329–340. Springer, Singapore (2018). https://link.springer.com/chapter/10.1007/978-981-10-5329-0_24

[19] Wang, S., Kreiss, G.: Convergence of summation-by-parts finite difference methods for the wave equation. J. Sci. Comput. **71**(1), 219–245 (2017)

[20] Svärd, M., Gong, J., Nordström, J.: An accuracy evaluation of unstructured node-centred finite volume methods. Appl. Numer. Math. **58**(8), 1142–1158 (2008) https://doi.org/10.1016/j.apnum.2007.05.002

[21] Neelan, A.G., Nair, M.: Hyperbolic Runge-Kutta method using evolutionary algorithm. J. Comput. Nonlin. Dynamics **13**(11) (2018) https://doi.org/10.1115/1.4040708

[22] Tysell, L., Nordström, J.: Accuracy evaluation of the unstructured node-centered finite volume method in aerodynamic computations. In: Proceedings of the 10th ISGG Conference on Numerical Grid Generation, International Society of Grid Generation (ISGG), Heraklion, Crete, Greece (2007)

[23] Eriksson, S., Nordström, J.: Analysis of mesh and boundary effects on the accuracy of node-centered finite volume schemes. In: 19th AIAA Computational Fluid Dynamics, p. 3651 (2009)

[24] Diskin, B., Thomas, J.L.: Comparison of node-centered and cell-centered unstructured finite-volume discretizations: inviscid fluxes. AIAA J. **49**(4), 836–854 (2011)

[25] Diskin, B., Thomas, J.L., Nielsen, E.J., Nishikawa, H., White, J.A.: Comparison of node-centered and cell-centered unstructured finite-volume discretizations: viscous fluxes. AIAA J. **48**(7), 1326–1338 (2010)

[26] Katz, A., Sankaran, V.: High aspect ratio grid effects on the accuracy of Navier–Stokes solutions on unstructured meshes. Comput. Fluids **65**, 66–79 (2012) https://doi.org/10.1016/j.compfluid.2012.02.012 . Sixth International Conference on Computational Fluid Dynamics (ICCFD6)

[27] Katz, A., Sankaran, V.: Mesh quality effects on the accuracy of CFD solutions on unstructured meshes. J. Comput. Phys. **230**(20), 7670–7686 (2011) https://doi.org/10.1016/j.jcp.2011.06.023

[28] Diskin, B., Thomas, J.L.: Notes on accuracy of finite-volume discretization schemes on irregular grids. Appl. Numer. Math. **60**(3), 224–226 (2010) https://doi.org/10.1016/j.apnum.2009.12.001

[29] Pulliam, T.H., Zingg, D.W.: Fundamental Algorithms in Computational Fluid Dynamics vol. 940. Springer, Cham, Switzerland (2014)

[30] Hermanns, M., Hernández, J.A.: Stable high-order finite-difference methods based on non-uniform grid point distributions. Int. J. Numer. Meth. Fluids **56**(3), 233–255 (2008) https://doi.org/10.1002/fld.1510 https://onlinelibrary.wiley.com/doi/pdf/10.1002/fld.1510

[31] Vasilyev, O.V.: High order finite difference schemes on non-uniform meshes with

good conservation properties. J. Comput. Phys. **157**(2), 746–761 (2000) https://doi.org/10.1006/jcph.1999.6398

[32] Shukla, R.K., Zhong, X.: Derivation of high-order compact finite difference schemes for non-uniform grid using polynomial interpolation. J. Comput. Phys. **204**(2), 404–429 (2005) https://doi.org/10.1016/j.jcp.2004.10.014

[33] Shukla, R.K., Tatineni, M., Zhong, X.: Very high-order compact finite difference schemes on non-uniform grids for incompressible Navier–Stokes equations. J. Comput. Phys. **224**(2), 1064–1094 (2007) https://doi.org/10.1016/j.jcp.2006.11.007

[34] Sharma, N., Sengupta, A., Rajpoot, M., Samuel, R.J., Sengupta, T.K.: Hybrid sixth order spatial discretization scheme for non-uniform Cartesian grids. Comput. Fluids **157**, 208–231 (2017) https://doi.org/10.1016/j.compfluid.2017.08.034

[35] Mishra, P., Gupta, V., Dubey, R.K.: A mesh adaptation algorithm using new monitor and estimator function for discontinuous and layered solution. Numer. Algebra Control Optim. **12**(3), 637–658 (2022) https://doi.org/10.3934/naco.2021029

[36] Dubey, R.K., Mishra, P.: Modified equation based mesh adaptation algorithm for evolutionary scalar partial differential equations. Numer. Methods Partial Differential Equations **39**(1), 108–132 (2023)

[37] Hoffmann, K.A.: Computational Fluid Dynamics for Engineers. Engineering education system, 100–103 (1993)

[38] Harten, A., Engquist, B., Osher, S., Chakravarthy, S.R.: Uniformly high order accurate essentially non-oscillatory schemes, III. J. Comput. Phys. **71**(2), 231–303 (1987) https://doi.org/10.1016/0021-9991(87)90031-3

[39] Liu, X.-D., Osher, S., Chan, T.: Weighted essentially non-oscillatory schemes. J. Comput. Phys. **115**(1), 200–212 (1994) https://doi.org/10.1006/jcph.1994.1187

[40] Jiang, G.-S., Shu, C.-W.: Efficient implementation of weighted ENO schemes. J. Comput. Phys. **126**(1), 202–228 (1996) https://doi.org/10.1006/jcph.1996.0130

[41] Kossaczká, T., Ehrhardt, M., Günther, M.: Enhanced fifth order WENO shock-capturing schemes with deep learning. Results Appl. Math. **12**, 100201 (2021) https://doi.org/10.1016/j.rinam.2021.100201

[42] Satyaprasad, D., Kuiry, S.N., Sundar, S.: A shock-capturing meshless method for solving the one-dimensional saint-venant equations on a highly variable topography. Journal of Hydroinformatics **25**(4), 1235–1255 (2023)

[43] Ghia, U., Ghia, K.N., Shin, C.T.: High-Re solutions for incompressible flow using the Navier-Stokes equations and a multigrid method. J. Comput. Phys. **48**(3), 387–411 (1982) https://doi.org/10.1016/0021-9991(82)90058-4

[44] Suman, V.K., Viknesh S., S., Tekriwal, M.K., Bhaumik, S., Sengupta, T.K.: Grid sensitivity and role of error in computing a lid-driven cavity problem. Phys. Rev. E **99**, 013305 (2019) https://doi.org/10.1103/PhysRevE.99.013305

[45] Taylor, G.I., Green, A.E.: Mechanism of the production of small eddies from large ones. Proc. Roy. Soc. London Ser. A Math. Phys. Sci. **158**(895), 499–521 (1937) https://doi.org/10.1098/rspa.1937.0036 https://royalsocietypublishing.org/doi/pdf/10.1098/rspa.1937.0036

[46] Sengupta, T.K., Sharma, N., Sengupta, A.: Non-linear instability analysis of the two-dimensional Navier-Stokes equation: The Taylor-Green vortex problem. Phys. Fluids **30**(5), 054105 (2018) https://doi.org/10.1063/1.5024765 https://doi.org/10.1063/1.5024765